ON TEMPERATURE SCALING AND CONFORMAL PREDICTION OF DEEP CLASSIFIERS

Anonymous authors
Paper under double-blind review

ABSTRACT

In many classification applications, the prediction of a deep neural network (DNN) based classifier needs to be accompanied by some confidence indication. Two popular approaches for that aim are: 1) *Calibration*: modifies the classifier's softmax values such that the maximal value better estimates the correctness probability; and 2) *Conformal Prediction* (CP): produces a prediction set of candidate labels that contains the true label with a user-specified probability, guaranteeing marginal coverage but not, e.g., per class coverage. In practice, both types of indications are desirable, yet, so far the interplay between them has not been investigated. Focusing on the ubiquitous *Temperature Scaling* (TS) calibration, we start this paper with an extensive empirical study of its effect on prominent CP methods. We show that while TS calibration improves the class-conditional coverage of adaptive CP methods, surprisingly, it negatively affects their prediction set sizes. Motivated by this behavior, we explore the effect of TS on CP *beyond its calibration application* and reveal an intriguing trend under which it allows to trade prediction set size and conditional coverage of adaptive CP methods. Then, we establish a mathematical theory that explains the entire non-monotonic trend. Finally, based on our experiments and theory, we offer simple guidelines for practitioners to effectively combine adaptive CP with calibration.

1 INTRODUCTION

Modern classification systems are typically based on deep neural networks (DNNs) (Krizhevsky et al., 2012; He et al., 2016; Huang et al., 2017). In many applications, it is necessary to quantify and convey the level of uncertainty associated with each prediction of the DNN. This is particularly crucial in high-stakes scenarios, such as medical diagnoses (Miotto et al., 2018), autonomous vehicle decision-making (Grigorescu et al., 2020), and detection of security threats (Guo et al., 2018), where human lives are at risk.

In practice, DNN classification models typically generate a post-softmax vector, akin to a probability vector with nonnegative entries that add up to one. One might, intuitively, be interested in using the value associated with the prediction as the confidence (Cosmides & Tooby, 1996). However, this value often deviates substantially from the actual correctness probability. This discrepancy, known as *miscalibration*, is prevalent in modern DNN classifiers, which frequently demonstrate overconfidence: the maximal softmax value surpasses the true correctness probability (Guo et al., 2017). To address this issue, post-processing *calibration* methods are employed to adjust the values of the softmax vector. In particular, Guo et al. (2017) demonstrated the usefulness of a simple Temperature Scaling (TS) procedure (a single parameter variant of Platt scaling (Platt et al., 1999)). Since then, TS calibration has gained massive popularity (Liang et al., 2018; Ji et al., 2019; Wang et al., 2021; Frenkel & Goldberger, 2021; Ding et al., 2021; Wei et al., 2022). Thus studying it is of high significance.

Another post-processing approach for uncertainty indication is Conformal Prediction (CP), which was originated in (Vovk et al., 1999; 2005) and has attracted much attention recently. CP algorithms are based on devising scores for all the classes per sample (based on the softmax values) that are used for producing a set of predictions instead of a single predicted class. These methods have theoretical guarantees for *marginal coverage*: given a user-specified probability, the produced set will contain the true label with this probability, assuming that the data samples are exchangeable (e.g., the samples

are i.i.d.). Note that this property does not ensure *conditional coverage*, i.e., coverage of the true label with the specified probability when conditioning the data, e.g., to a specific class. Consequently, CP methods are usually compared by both their prediction set sizes and their conditional coverage performance.

Clearly, in critical applications, both calibration and CP are desirable, as they provide complementary types of information that can lead to a comprehensive decision. However, as far as we know, so far the interplay between them has not been investigated. Specifically, the works (Angelopoulos et al., 2021; Lu et al., 2022; Gibbs et al., 2023; Lu et al., 2023) apply initial *TS calibration* (rather than any other calibration method) before applying their CP methods. Yet, none of them investigates what is the effect of this procedure on the CP methods.

In this work, we study the effect of TS, arguably the most common calibration technique, on three prominent CP methods: Least Ambiguous set-valued classifier (LAC) (Lei & Wasserman, 2014; Sadinle et al., 2019), Adaptive Prediction Sets (APS) (Romano et al., 2020), and Regularized Adaptive Prediction Sets (RAPS) (Angelopoulos et al., 2021). Note that LAC (aka THR), APS and RAPS are probably the three most popular CP methods for classification. Indeed, important papers in this field, such as (Angelopoulos et al., 2021) and (Stutz et al., 2022), do not consider any other CP method. Our discoveries on the effect of TS calibration in this paper have motivated us to explore the TS mechanism also beyond its calibration application.

Our contributions can be summarized as follows:

- We conduct an extensive empirical study on DNN classifiers that shows that an initial TS calibration affects CP methods differently. Specifically, we show that its effect is negligible for LAC, but intriguing for adaptive methods (APS and RAPS): while their class-conditional coverage is improved, surprisingly, their prediction set sizes typically become larger.
- Following these findings, we investigate the impact of TS on CP *for a wide range of temperatures, beyond the values used for calibration*. We reveal that by modifying the temperature, TS enables to trade the prediction set sizes and the class-conditional coverage performance for RAPS and APS. Moreover, metrics of these properties display a similar non-monotonic pattern across all models and datasets examined.
- We present a rigorous theoretical analysis of the impact of TS on the prediction set sizes of APS and RAPS, offering a comprehensive explanation for the complex non-monotonic patterns observed empirically.
- Based on our theoretically-backed findings, we propose practical guidelines to effectively combine adaptive CP methods with TS calibration, which allow users to control the prediction set sizes and conditional coverage trade-off.

2 Background and Related Work

Let us present the notations that are used in the paper, followed by some preliminaries on TS and CP. We consider a C-classes classification task of the data (X, Y) distributed on $\mathbb{R}^d \times [C]$, where $[C] := \{1, \ldots, C\}$. The classification is tackled by a DNN that for each input sample $\mathbf{x} \in \mathbb{R}^d$ produces a logits vector $\mathbf{z} = \mathbf{z}(\mathbf{x}) \in \mathbb{R}^C$ that is fed into a final softmax function $\boldsymbol{\sigma} : \mathbb{R}^C \to \mathbb{R}^C$, defined as $\sigma_i(\mathbf{z}) = \dfrac{\exp(z_i)}{\sum_{j=1}^{C} \exp(z_j)}$. Typically, the post-softmax vector $\hat{\boldsymbol{\pi}}(\mathbf{x}) = \boldsymbol{\sigma}(\mathbf{z}(\mathbf{x}))$ is being treated as an estimate of the class probabilities. The predicted class is given by $\hat{y}(\mathbf{x}) = \operatorname{argmax}_i \hat{\pi}_i(\mathbf{x})$.

2.1 Calibration and Temperature Scaling

The interpretation of $\hat{\boldsymbol{\pi}}(\mathbf{x})$ as an estimated class probabilities vector promotes treating $\hat{\pi}_{\hat{y}(\mathbf{x})}(\mathbf{x})$ as the probability that the predicted class $\hat{y}(\mathbf{x})$ is correct, also referred to as the model's *confidence*. However, it has been shown that DNNs are frequently overconfident — $\hat{\pi}_{\hat{y}(x)}(x)$ is larger than the true correctness probability (Guo et al., 2017). Formally, $\mathbb{P}\left(\hat{y}(X) = Y | \hat{\pi}_{\hat{y}(X)}(X) = p\right) < p$ with significant margin. Post-processing calibration techniques aim at reducing the aforementioned gap. They are based on optimizing certain transformations of the logits $\mathbf{z}(\cdot)$, yielding a probability

vector $\tilde{\boldsymbol{\pi}}(\cdot)$ that minimizes an objective computed over a dedicated *calibration set* of labeled samples $\{\mathbf{x}_i, y_i\}_{i=1}^n$ (Platt et al., 1999; Zadrozny & Elkan, 2002; Naeini et al., 2015; Nixon et al., 2019). Two popular calibration objectives are the Negative Log-Likelihood (NLL) (Hastie et al., 2005) and the Expected Calibration Error (ECE) (Naeini et al., 2015), detailed in Appendix B.3.

Temperature Scaling (TS) (Guo et al., 2017) stands out as, arguably, the most common calibration approach, surpassing many others in achieving calibration with minimal computational complexity (Liang et al., 2018; Ji et al., 2019; Wang et al., 2021; Frenkel & Goldberger, 2021; Ding et al., 2021; Wei et al., 2022). It simply uses the transformation $\mathbf{z} \mapsto \mathbf{z}/T$ before applying the softmax, where $T > 0$ (the *temperature*) is a single scalar parameter that is set by minimizing NLL or ECE. Additionally, TS preserves the accuracy rate of the network (the ranking of the elements – and in particular, the index of the maximum – is unchanged), which may otherwise be compromised during the calibration phase.

Hereafter, we use the notation $\hat{\boldsymbol{\pi}}_T(\mathbf{x}) := \boldsymbol{\sigma}(\mathbf{z}(\mathbf{x})/T)$ to denote the output of the softmax when taking into account the temperature. Observe that $T = 1$ preserves the original probability vector. Let us denote by T^* the temperature that is optimal for TS calibration. Since DNN classifiers are commonly overconfident, TS calibration typically yields some $T^* > 1$, which "softens" the original probability vector. Formally, TS with $T > 1$ raises the entropy of the softmax output (formally shown in Proposition A.5 in the appendix).

The *reliability diagram* (DeGroot & Fienberg, 1983; Niculescu-Mizil & Caruana, 2005) is a graphical depiction of a model before and after calibration. The confidence range $[0, 1]$ is divided into bins and the validation samples (not used in the calibration) are assigned to the bins according to $\hat{\pi}_{\hat{y}(\mathbf{x})}(\mathbf{x})$. The average accuracy (Top-1) is computed per bin. In the case of perfect calibration, the diagram should be aligned with the identity function. Any significant deviation from slope of 1 indicates miscalibration. In Appendix B.4.1, we provide reliability diagrams for the dataset-model pairs examined in our study.

2.2 Conformal Prediction

Conformal Prediction (CP) is a methodology that is model-agnostic and distribution-free, designed for generating a *prediction set* of classes $\mathcal{C}_\alpha(X)$ for a given sample X, such that $Y \in \mathcal{C}_\alpha(X)$ with probability $1 - \alpha$ for a predefined $\alpha \in (0, 1)$, where Y is the true class associated with X (Vovk et al., 1999; 2005; Papadopoulos et al., 2002). The decision rule is based on a calibration set of labeled samples $\{\mathbf{x}_i, y_i\}_{i=1}^n$, which we hereafter refer to as the *CP set*, to avoid confusion with the set used for TS calibration. The only assumption in CP is that the random variables associated with the CP set and the test samples are exchangeable (e.g., the samples are i.i.d.).

Let us state the general process of conformal prediction given the CP set $\{\mathbf{x}_i, y_i\}_{i=1}^n$ and its deployment for a new (test) sample x_{n+1} (for which y_{n+1} is unknown), as presented in (Angelopoulos & Bates, 2021):

1. Define a heuristic score function $s(\mathbf{x}, y) \in \mathbb{R}$ based on some output of the model. A higher score should encode a lower level of agreement between $\mathbf{x}$ and y.
2. Compute $\hat{q}$ as the $\dfrac{\lceil (n+1)(1-\alpha) \rceil}{n}$ quantile of the scores $\{s(\mathbf{x}_1, y_1), \ldots, s(\mathbf{x}_n, y_n)\}$.
3. At deployment, use $\hat{q}$ to create prediction sets for new samples: $\mathcal{C}_\alpha(\mathbf{x}_{n+1}) = \{y : s(\mathbf{x}_{n+1}, y) \leq \hat{q}\}$.

CP methods possess the following coverage guarantee.

Theorem 2.1 (Theorem 1 in (Angelopoulos & Bates, 2021)). *Suppose that $\{(X_i, Y_i)\}_{i=1}^n$ and (X_{n+1}, Y_{n+1}) are i.i.d., and define $\hat{q}$ as in step 2 above and $\mathcal{C}_\alpha(X_{n+1})$ as in step 3 above. Then the following holds:*

$$\mathbb{P}\left(Y_{n+1} \in \mathcal{C}_\alpha(X_{n+1})\right) \geq 1 - \alpha. \tag{1}$$

The proof of this result is based on (Vovk et al., 1999). A proof of an upper bound of $1-\alpha+1/(n+1)$ also exists. This property is called *marginal coverage* since the probability is taken over the entire distribution of (X, Y).

While achieving marginal coverage is practically feasible, it unfortunately does not imply the much more stringent property of *conditional coverage*:

$$\mathbb{P}\left(Y_{n+1} \in \mathcal{C}_\alpha(X_{n+1}) | X_{n+1} = \mathbf{x}\right) \geq 1 - \alpha. \tag{2}$$

Yet, coverage for any value $\mathbf{x}$ of the random X is impracticable (Vovk, 2012), (Foygel Barber et al., 2021), and a useful intuitive relaxation is to consider class-conditional coverage.

CP methods are usually compared by the size of their prediction sets and by their proximity to the conditional coverage property. Over time, various CP techniques with distinct objectives have been developed (Angelopoulos & Bates, 2021). There have been also efforts to alleviate the exchangeability assumption (Tibshirani et al., 2019; Barber et al., 2023). In this paper we will focus on three prominent CP methods. Each of them devises a different score $s(\mathbf{x}, y)$ based on the output of the classifier's softmax $\hat{\boldsymbol{\pi}}(\cdot)$.

Least Ambiguous Set-valued Classifier (LAC) (Lei & Wasserman, 2014; Sadinle et al., 2019). In this method, $s(\mathbf{x}, y) = 1 - \hat{\pi}_y(\mathbf{x})$. Accordingly, given $\hat{q}_{LAC}$ associated with α through step 2, the prediction sets are formed as: $\mathcal{C}^{LAC}(\mathbf{x}) := \{y : \hat{\pi}_y(\mathbf{x}) \geq 1 - \hat{q}_{LAC}\}$. LAC tends to have small set sizes (under the strong assumption that $\hat{\boldsymbol{\pi}}(\mathbf{x})$ matches the posterior probability, it provably gives the smallest possible average set size). On the other hand, its conditional coverage is limited.

Adaptive Prediction Sets (APS) (Romano et al., 2020). The objective of this method is to improve the conditional coverage. Motivated by theory derived under the strong assumption that $\hat{\boldsymbol{\pi}}(\mathbf{x})$ matches the posterior probability, it uses $s(\mathbf{x}, y) = \sum_{i=1}^{L_y} \hat{\pi}_{(i)}(\mathbf{x})$, where $\hat{\pi}_{(i)}(\mathbf{x})$ denotes the i-th element in a descendingly sorted version of $\hat{\boldsymbol{\pi}}(\mathbf{x})$ and L_y is the index that y is permuted to after sorting. Following steps 2 and 3, yields $\hat{q}_{APS}$ and $\mathcal{C}^{APS}(\mathbf{x})$.

Regularized Adaptive Prediction Sets (RAPS) (Angelopoulos et al., 2021). A modification of APS that aims at improving its prediction set sizes by penalizing hard examples to reduce their effect on $\hat{q}$. With the same notation as APS, in RAPS we have $s(\mathbf{x}, y) = \sum_{i=1}^{L_y} \hat{\pi}_{(i)}(\mathbf{x}) + \lambda(L_y - k_{reg})_+$, where $\lambda, k_{reg} \geq 0$ are regularization hyperparameters and we use the notation $(\cdot)_+ := \max\{\cdot, 0\}$. Following steps 2 and 3, yields $\hat{q}_{RAPS}$ and $\mathcal{C}^{RAPS}(\mathbf{x})$.

Note that all these CP methods can be readily applied on $\boldsymbol{\pi}_{T^*}(\cdot)$ after TS calibration. This is done, in (Angelopoulos et al., 2021; Lu et al., 2022; Gibbs et al., 2023; Lu et al., 2023), where the authors stated that they applied TS calibration before examining the CP techniques. However, none of these works has examined how TS calibration impacts any CP method. All the more so, no existing work has experimented applying TS with a range of temperatures before employing CP methods.

3 The Effect of TS on CP Methods for DNN Classifiers

In this section, we empirically investigate the effect of TS on the performance of CP algorithms. Specifically, we consider different datasets and models, and start by reporting the mean prediction set size, marginal coverage, and class-conditional coverage of CP algorithms, with and without an initial TS calibration procedure. Then, we extend the empirical study to encompass a wide range of temperatures and discuss our findings.

3.1 Experimental setup

Datasets. We conducted our experiment on CIFAR-10, CIFAR-100 (Krizhevsky et al., 2009) and ImageNet (Deng et al., 2009) chosen for their diverse content and varying levels of difficulty.

Models. We utilized a diverse set of DNN classifiers, based on ResNets (He et al., 2016), DenseNets (Huang et al., 2017) and ViT (Dosovitskiy et al., 2021).

For CIFAR-10: ResNet34 and ResNet50. For CIFAR-100: ResNet50 and DenseNet121. For ImageNet: ResNet152, DenseNet121 and ViT-B/16. Details on the training of the models are provided in Appendix B.1.

TS calibration. For each dataset-model pair, we create a calibration set by randomly selecting 10% of the validation set. We obtain the calibration temperature T^* by optimizing the ECE objective. The

Table 1: **Prediction Set Size.** AvgSize metric along with T^* and accuracy for dataset-model pairs using LAC, APS, and RAPS algorithms with $\alpha = 0.1$, CP set size 10%, pre- and post-TS calibration.

		Accuracy(%)		**AvgSize**			**AvgSize after TS**		
Dataset-Model	T^*	Top-1	Top-5	LAC	APS	RAPS	LAC	APS	RAPS
ImageNet, ResNet152	1.227	78.3	94.0	1.95	6.34	2.71	1.92	11.11	4.30
ImageNet, DenseNet121	1.024	74.4	91.9	2.73	9.60	4.70	2.76	11.32	4.88
ImageNet, ViT-B/16	1.180	83.9	97.0	2.22	10.10	1.93	2.23	19.27	2.34
CIFAR-100, ResNet50	1.524	80.9	95.4	1.62	5.31	2.88	1.57	9.14	4.96
CIFAR-100, DenseNet121	1.469	76.1	93.5	2.13	4.26	2.98	2.06	6.51	4.27
CIFAR-10, ResNet50	1.761	94.6	99.7	0.91	1.04	0.98	0.91	1.13	1.05
CIFAR-10, ResNet34	1.802	95.3	99.8	0.91	1.03	0.94	0.93	1.11	1.05

Table 2: **Coverage Metrics.** MarCovGap and TopCovGap metrics for dataset-model pairs using LAC, APS, and RAPS algorithms with $\alpha = 0.1$, CP set size 10%, pre- and post-TS calibration.

	MarCovGap(%)			**MarCovGap TS(%)**			**TopCovGap(%)**			**TopCovGap TS(%)**		
Dataset-Model	LAC	APS	RAPS	LAC	APS	RAPS	LAC	APS	RAPS	LAC	APS	RAPS
ImageNet, ResNet152	0.1	0	0	0	0	0	23.1	16.0	17.6	23.9	13.8	15.2
ImageNet, DenseNet121	0	0.1	0	0.1	0	0	24.9	15.7	18.0	25.2	14.9	17.6
ImageNet, ViT-B/16	0	0	0	0.1	0.1	0	24.8	14.2	14.7	24.9	12.2	12.5
CIFAR-100, ResNet50	0.1	0	0	0	0.1	0	13.9	12.6	11.7	12.9	9.0	7.9
CIFAR-100, DenseNet121	0	0	0	0	0	0.1	11.5	9.5	9.7	12.2	7.8	8.0
CIFAR-10, ResNet50	0	0	0	0	0.1	0	11.1	5.0	4.8	11.2	2.4	2.6
CIFAR-10, ResNet34	0	0	0.1	0	0	0	9.5	3.0	2.8	9.1	2.2	2.2

optimal temperatures when using the NLL objective are very similar, as displayed in Table 3 in the Appendix B.3.1. This justifies using ECE as the default for the experiments.

CP Algorithms. For each of the dataset-model pairs, we construct the "CP set" (used for computing the thresholds of CP methods) by randomly selecting $\{5\%, 10\%, 20\%\}$ of the validation set, while ensuring not to include in the CP set samples that are used in the TS calibration. The CP methods that we examine are LAC, APS, and RAPS, detailed in Section 2.2 (we use the randomized versions of APS and RAPS, as done in (Angelopoulos et al., 2021)). For each technique, we use $\alpha = 0.1$ and $\alpha = 0.05$, so the desired marginal coverage probability is 90% and 95%, as common in most CP literature (Romano et al., 2020; Angelopoulos et al., 2021; Angelopoulos & Bates, 2021).

Metrics. We report metrics over the validation set samples that were not included in the calibration set or CP set. The metrics are as follows:

• *Average set size* (AvgSize) - The mean prediction set size of the CP algorithm. (See equation 15 for the definition.)
• *Marginal coverage gap* (MarCovGap) - The deviation of the marginal coverage from the desired $1 - \alpha$. (See equation 16 for the definition.)
• *Top-5% class-coverage gap* (TopCovGap) - The deviation from the desired $1-\alpha$ coverage, averaged over the 5% of classes with the highest deviation. We use top-5% classes deviation due to the high variance in the maximal class deviation. (See equation 17 for the definition.)

The mathematical definitions of the metrics, along with additional details about the experimental setup, are presented in Appendix B.4. Note that for these metrics: *the lower the better*. Similar metrics have been used in (Ding et al., 2023; Angelopoulos et al., 2021). All the reported results, per metric, are the median-of-means along 100 trials where we randomly select the calibration/CP sets, similarly to (Angelopoulos et al., 2021).

3.2 The effect of TS calibration on CP methods

For each of the dataset-model pairs we compute the aforementioned metrics with and without an initial TS calibration procedure. In Table 1, we report the the calibration temperature T^*, the accuracy (not affected by TS), and the median-of-means of the prediction set sizes metric, AvgSize. In Table 2, we report the median-of-means of the marginal and conditional coverage metrics, MarCovGap and TopCovGap. In both tables, the specified coverage probability is 90% ($\alpha = 0.1$), and we use 10% of the samples for the CP set and 10% of the samples for the calibration set. Due to space limitation, the results for coverage probability of 95% ($\alpha = 0.05$) and sizes $\{5\%, 20\%\}$ of the CP sets are deffer to Appendix B.5. The insights gained from Tables 1 and 2 hold also for the deferred results.

Examining the results, we first see that the TS calibration temperatures, T^*, in Table 1 are greater than 1, indicating that the models exhibit overconfidence. The reliability diagrams before and after TS calibration are presented in Appendix B.4.1.

By examining MarCovGap in Table 2, we see that all CP methods maintain marginal coverage both with and without the initial TS procedure (the gap is at most 0.1%, i.e., 0.001). That is, TS calibration does not affect this property, which is consistent with CP theoretical guarantees (Theorem 2.1).

As for the conditional coverage, as indicated by the TopCovGap metric in Table 2, there is no distinct trend observed for the LAC method. On the other hand, in the adaptive CP methods, APS and RAPS, there is a noticeable improvement (TopCovGap decreases), especially when T^* is high. We turn to examine Table 1, which reports the effect of TS calibration on the prediction set size of the CP methods. First, we see that for the CIFAR-10, where the models' accuracy is very high, the effect on AvgSize is minor. Second, we see that the effect on LAC is negligible also for other datasets. (Note that while LAC has lower AvgSize than APS and RAPS, its conditional coverage is worse, as shown by TopCovGap in Table 2). Third, perhaps the most thought provoking observation, for APS and RAPS the TS calibration procedure has led to *increase* in the mean prediction set size. Especially, when the value of the optimal temperature T^* is high. For instance, for ResNet50 on CIFAR-100, TS calibration increases AvgSize of APS from 5.31 to 9.14. This behavior is quite surprising.

In order to verify that the increase in the mean set size for APS and RAPS is not caused by a small number of extreme outliers, we "microscopically" analyze the change per sample. Specifically, for each sample in the validation set, we compare the prediction set size after the CP procedure with and without the initial TS calibration (i.e., set size with TS calibration minus set size without). Sorting the differences in a descending order yields a staircase-shaped curve. The smoothed version of this curve, which is obtained after averaging over the 100 trials, is presented in Figure 1 for ResNet50 trained on CIFAR-100, both for APS and for RAPS. Similar behavior is observed for other dataset-model pairs, as displayed by the figures in Appendix B.5.

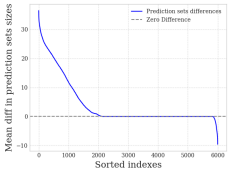

CIFAR100, ResNet50, APS

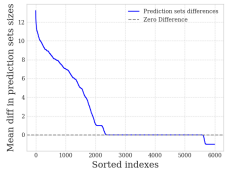

CIFAR100, ResNet50, RAPS

Figure 1: Mean sorted differences in prediction set sizes before and after TS calibration. More samples exhibit an increase than a decrease, and the extent of the increase is greater.

In Figure 1, approximately one third of the samples experience a negative impact on the prediction set size due to the TS calibration. For about half of the samples, there is no change in set size. Only the remaining small minority of samples experience improvement but to a much lesser extent than the harm observed for others. Interestingly, the existence of samples (though few) where the TS procedure causes a decrease in set size indicates that we cannot make a universal (uniform) statement about the impact of TS on the set size of arbitrary sample, but rather consider a typical/average case.

3.3 TS BEYOND CALIBRATION

The intriguing observations regarding TS calibration — especially, *both positively and negatively affecting different aspects of APS and RAPS* — prompt us to explore the effects of TS on CP, beyond calibration. In Figure 2 we present the average prediction set size, AvgSize, the class-conditional coverage metric, TopCovGap, and the threshold value of the CP methods, $\hat{q}$, for temperatures ranging from 0.5 to 5 with an increment of 0.1. The reported results are the median-of-means for 100 trials. We present here three diverse dataset-model pairs, and defer the others to Appendix B.6 due to space limitation. The appendix also includes different settings, such as various calibration set sizes and coverage probability levels, detailed in Section 3.1.

Figure 2 displays interesting non-monotonic trends of AvgSize and TopCovGap for APS and RAPS. Across all dataset-model combinations, these metrics exhibit similar patterns: AvgSize (top row) increases until reaching a peak, and then starts declining; TopCovGap (middle row) decreases until reaching a minimum, then reverses and starts increasing. The threshold value $\hat{q}$ (bottom row), on the other hand, decreases monotonically for APS and RAPS. For LAC no clear pattern is evident.

If we restrict our view to, e.g., $T < T_{critical}$ (before AvgSize reaches the peak), we see generalization of the observations in the TS calibration experiments in Section 3.2. Specifically, for the APS and RAPS algorithms, as T increases AvgSize increases while TopCovGap decreases. This reveals that in this range of T, there is a *trade-off* between the two crucial properties of APS and RAPS – prediction set sizes and conditional coverage – which can be controlled by increasing/decreasing T.

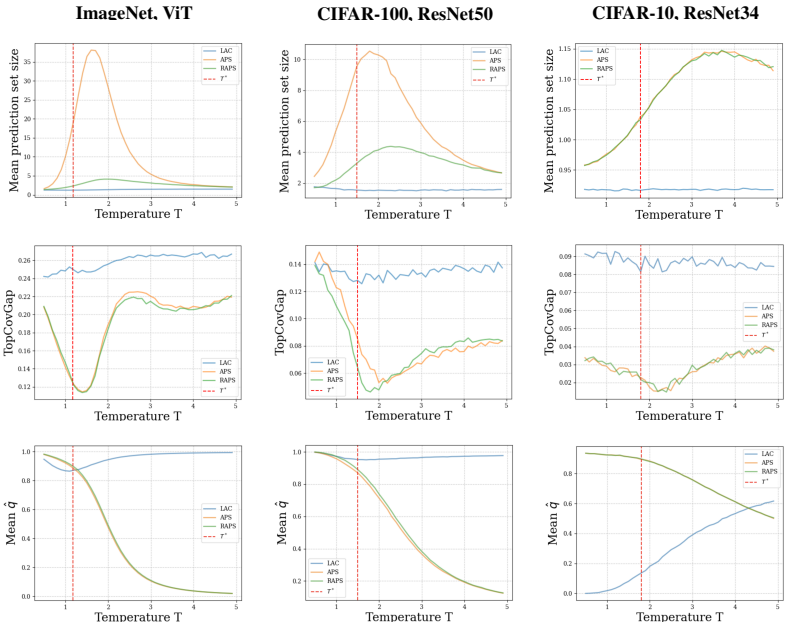

Figure 2: AvgSize (top), TopCovGap (middle), and mean threshold $\hat{q}$ (bottom) for LAC, APS and RAPS with $\alpha = 0.1$ versus the temperature T. The vertical line marks T^* obtained by calibration.

In fact, overall, the trade-off remains also beyond the maximum/minimum of AvgSize/TopCovGap. Nevertheless, the existence of the extreme points is surprising and not intuitive.

4 Theoretical Analysis

In this section, we provide mathematical reasoning for empirical observations regarding the effect of TS on the prediction set size of APS and RAPS presented in Section 3. Theoretically analyzing our other findings, such as the effect of TS on the conditional coverage, are left for future research. *All the proofs are provided in Appendix A.*

4.1 The threshold of APS and RAPS decreases as T increases

In Section 3.3, we observe that increasing the temperature monotonically reduces the threshold of APS and RAPS. Let us prove this theoretically. Later, we will use this result in our theory on the effect of TS on the prediction set size.

Let $\mathbf{z} = \mathbf{z}(\mathbf{x})$ be the logits vector of a sample $\mathbf{x}$. Let $\hat{\boldsymbol{\pi}}_T = \boldsymbol{\sigma}(\mathbf{z}/T)$ be the softmax vector after TS with temperature T. We denote by $s_T(\mathbf{x}, y)$ the score of the APS method when applied on $\hat{\boldsymbol{\pi}}_T$. Namely, $s_T(\mathbf{x}, y) = \sum_{i=1}^{L_y} \hat{\pi}_{T,(i)}$, where $\hat{\pi}_{T,(i)}$ denotes the i-th element in a descendingly sorted version of $\hat{\boldsymbol{\pi}}_T$ and L_y is the index that y is permuted to after sorting. Recall that the RAPS algorithm is based on the same score with an additional regularization term that is not affected by TS.

The following theorem states that a cumulative sum of a sorted softmax vector, analogous to the APS score, decreases as the temperature T increases.

Theorem 4.1. *Let $\mathbf{z} \in \mathbb{R}^C$ be a sorted logits vector, i.e., $z_1 \geq z_2 \geq \ldots \geq z_C$, and let $L \in [C]$. Let $\hat{\boldsymbol{\pi}}_T = \boldsymbol{\sigma}(\mathbf{z}/T)$ and $\hat{\boldsymbol{\pi}}_{\tilde{T}} = \boldsymbol{\sigma}(\mathbf{z}/\tilde{T})$ with $T > \tilde{T} > 0$. Then, we have $\sum_{j=1}^{L} \pi_{\tilde{T},j} \geq \sum_{j=1}^{L} \pi_{T,j}$. The inequality is strict, unless $L = C$ or $z_1 = \ldots = z_C$.*

Note that Theorem 4.1 is universal: it holds for any sorted logits vector. Denote the threshold obtained by applying the CP method after TS by $\hat{q}_T$. Based on the universality of the theorem, we can establish that increasing the temperature T decreases $\hat{q}_T$ for APS and RAPS.

Corollary 4.2. *The threshold value $\hat{q}_T$ of APS and RAPS decreases monotonically as T increases.*

4.2 THE EFFECT OF TS ON PREDICTION SET SIZES OF APS

In Section 3.3, we observe a consistent dependency on the temperature parameter T across all models and datasets: the mean prediction set size of APS and RAPS switches from increasing to decreasing as T passes some value $T_{critical}$. In this section, we provide a theoretical analysis to elucidate this behavior. For simplification we focus on APS.

Let $\hat{q}_T$ and $\hat{q}$ denote the thresholds of APS when applied with and without TS, respectively. For a new test sample $\mathbf{x}$ with logits vector $\mathbf{z}$ that is *sorted in descending order*, $\hat{\boldsymbol{\pi}}_T = \boldsymbol{\sigma}(\mathbf{z}/T)$ and $\hat{\boldsymbol{\pi}} = \boldsymbol{\sigma}(\mathbf{z})$ are the softmax outputs with and without TS, which are *sorted as well*. We denote $L_T = \min\{l : \sum_{i=1}^{l} \hat{\pi}_{T,i} \geq \hat{q}_T\}$, $L = \min\{l : \sum_{i=1}^{l} \hat{\pi}_i \geq \hat{q}\}$ as the prediction set sizes for this sample according to APS with and without TS, respectively.

We aim to investigate the conditions under which the events $L_T \geq L$ and $L_T \leq L$ occur. Since analyzing these events directly seems to be challenging, we leverage the following proposition that establishes alternative events that are sufficient conditions.

Proposition 4.3. *Let $\mathbf{z} \in \mathbb{R}^C$ such that $z_1 \geq z_2 \geq \cdots \geq z_C$, $\hat{\boldsymbol{\pi}}_T = \boldsymbol{\sigma}(\mathbf{z}/T)$ and $\hat{\boldsymbol{\pi}} = \boldsymbol{\sigma}(\mathbf{z})$. Let $\hat{q}, \hat{q}_T \in (0, 1]$ such that if $T > 1$ then $\hat{q} \geq \hat{q}_T$ and if $0 < T < 1$ then $\hat{q} \leq \hat{q}_T$. Let $L = \min\{l : \sum_{i=1}^{l} \hat{\pi}_i \geq \hat{q}\}$, $L_T = \min\{l : \sum_{i=1}^{l} \hat{\pi}_{T,i} \geq \hat{q}_T\}$. The following holds:*

$$\begin{cases} \textit{If} \quad 0 < T < 1, \quad \textit{then}: \quad \forall M \in [L]: \quad \sum_{i=1}^{M} \hat{\pi}_i - \sum_{i=1}^{M} \hat{\pi}_{T,i} \leq \hat{q} - \hat{q}_T \implies L \geq L_T \\ \textit{If} \quad T > 1, \quad \textit{then}: \quad \forall M \in [L]: \quad \sum_{i=1}^{M} \hat{\pi}_i - \sum_{i=1}^{M} \hat{\pi}_{T,i} \geq \hat{q} - \hat{q}_T \implies L \leq L_T \end{cases} \tag{3}$$

The right-hand side of the new inequalities pertains to the difference between the threshold values before and after applying TS. Analyzing this term requires understanding the properties of the quantile sample of APS.

Let $\mathbf{z}^q$ and $\boldsymbol{\pi}^q$ denote the sorted logits vector and the softmax vector associated with the sample associated with APS threshold (without applying TS), that we dub "the quantile sample". The CP theory builds on the quantile sample being larger than $(1-\alpha)\%$ of the scores of other samples with high probability. As illustrated in Figure 3, beyond a certain score threshold, there is a strong correlation between the score value and the difference $\Delta z := z_{(1)} - z_{(2)}$. This implies that, for typical values of α (e.g., 0.1), the quantile sample exhibits a highly dominant first entry in its softmax vector, i.e., $\pi^q_{(1)} \gg \pi^q_{(2)}$ (recall that $\pi_i = \exp(z_i)/c$ where c is the denominator of the softmax shared by all entries). Similar behaviour occurs with TS calibration, see Figure 3. Thus, if we denote $\mathbf{z}^q_T$ and $\boldsymbol{\pi}^q_T$ as the quantile sample when TS is used, we still have $\pi^q_{T,(1)} \gg \pi^q_{T,(2)}$. Consequently, $\boldsymbol{\pi}^q \approx \boldsymbol{\pi}^q_T$. Therefore, it is reasonable to make the technical assumption that both $\hat{q}$ and $\hat{q}_T$ correspond to the same sample in the CP set, denoted here by the sorted logits vector $\mathbf{z}^q$.

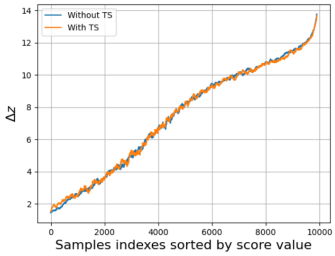

Figure 3: Δz for each sample sorted by score value (from low to high) with and without TS calibration, for CIFAR100-ResNet50.

For the rest of the analysis, we define the "gap function" as follows:

$$g(\mathbf{z}; T, M) = \sum_{i=1}^{M} \sigma_i(\mathbf{z}) - \sum_{i=1}^{M} \sigma_i(\mathbf{z}/T) = \frac{\sum_{i=1}^{M} \exp(z_i)}{\sum_{j=1}^{C} \exp(z_j)} - \frac{\sum_{i=1}^{M} \exp(z_i/T)}{\sum_{j=1}^{C} \exp(z_j/T)} \tag{4}$$

where $\mathbf{z}$ is a logits vector sorted in descending order.

With our assumption that $\hat{q}$ and $\hat{q}_T$ are associated with the same quantile sample $\mathbf{z}^q$, we have that $\hat{q} - \hat{q}_T$ in equation 3 can be written as $g(\mathbf{z}^q; T, L^q)$, where L^q denotes the rank of the true label of $\mathbf{z}^q$. Empirically, we observed that $g(\mathbf{z}^q, T, M) \approx g(\mathbf{z}^q, T, L^q)$ in our experiments (where $\Delta z^q = z^q_{(1)} - z^q_{(2)} \gg 1$). Furthermore, in Proposition A.6, we prove that $|g(\mathbf{z}^q, T, M) - g(\mathbf{z}^q, T, L^q)|$ decays exponentially with Δz^q. See Appendix A.1 for more details. This justifies studying the

following events:

$$\begin{cases} g(\mathbf{z};T,M) \leq g(\mathbf{z}^q;T,M) & \text{if } \ 0<T<1 \\ g(\mathbf{z};T,M) \geq g(\mathbf{z}^q;T,M) & \text{if } \ T>1 \end{cases} \tag{5}$$

Returning to consider $\mathbf{z}$ as the sorted logits vector of a test sample, typically it has lower score than the quantile sample $\mathbf{z}^q$, and thus as illustrated in Figure 3 also lower Δz. Consequently, it is intuitive to associate an increase in the score with an increase in the first entry of the sorted logits vector, z_1. We now present our key theorem that establishes a connection between the difference Δz and the sign of $\nabla_{z_1} g(\mathbf{z};T,M)$, depending on T.

Theorem 4.4. *Let $\mathbf{z} \in \mathbb{R}^C$ such that $z_1 \geq z_2 \geq \cdots \geq z_C$ and denote $\Delta z = z_1 - z_2$. Then, the following holds:*

$$\begin{cases} \textit{If} \quad 0<T<1: \quad \Delta z > \max\left\{ \dfrac{T}{T-1}\ln\left(\dfrac{T}{4}\right), \dfrac{T}{T+1}\ln\left(\dfrac{4(C-1)^2}{T}\right) \right\} \implies \nabla_{z_1} g(\mathbf{z};T,M) > 0 \\ \textit{If} \quad T>1: \quad \Delta z > \max\left\{ \dfrac{T}{T-1}\ln(4T), \dfrac{T-1}{T+1}\ln(4T(C-1)^2) \right\} \implies \nabla_{z_1} g(\mathbf{z};T,M) < 0 \end{cases} \tag{6}$$

Denote the lower bounds in Theorem 4.4 as $b_{T<1}(T)$ and $b_{T>1}(T)$. Let us consider the case of TS with $T>1$. The theorem establishes that for a sample with a sorted logits vector $\mathbf{z}$ satisfying $\Delta z > b_{T>1}(T)$, we have that $g(\mathbf{z})$ decreases monotonically as z_1 increases (indeed, when z_1 increases then Δz increases, and thus the inequality $\Delta z > b_{T>1}(T)$ remains satisfied). Since $\mathbf{z}^q$ has larger dominant entry than typical $\mathbf{z}$, this implies that $g(\mathbf{z};T,M) > g(\mathbf{z}^q;T,M)$. Thus, under our single technical assumption that $\hat{q}$ and $\hat{q}_T$ correspond to the same sample, we can apply Proposition 4.3 and get $L_T \geq L$ — a larger prediction set of APS. Conversely, by the same logic, the effect of TS with $0<T<1$ on a sample with a sorted logits vector $\mathbf{z}$ satisfying $\Delta z > b_{T<1}(T)$, is a smaller prediction set of APS.

We now show that the bounds in Theorem 4.4 do not require unreasonable values of Δz and T. In particular, the theorem explains the phenomenon for a "typical" $\mathbf{z}$ — e.g., the sample with the median score in Figure 3 — which in turn explains why we see the increase/decrease of the *mean* prediction set. Indeed, for this sample, according to Figure 3 we have $\Delta z \approx 8$. For $C=100$ (as in this CIFAR-100 experiment), the bounds in the theorem are complied by this sample for the temperature ranges $0<T<0.831$ and $1.25<T<4.81$. Since the calibrated temperature in this CIFAR100-ResNet50 experiment is $T^*=1.524$, which falls in this range, we rigorously proved increased prediction set for the median sample after TS calibration. Interestingly, the broad temperature range that is covered by our theory indicates that our bounds are sufficiently tight to establish additional fine-grained insights.

Implications of the theorem's bounds. To demonstrate the significance of our theory, we analyze the bounds established in Theorem 4.4, unitedly denoted as $b(T), T>0$. We leverage our theory to explain the entire non-monotonic trend in the empirical results on the effect of TS on the mean prediction set size of APS (and the closely related RAPS), showed in Figure 2.

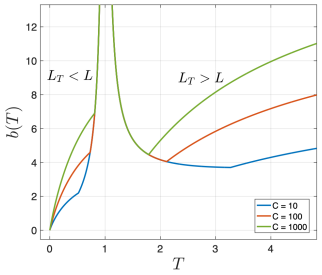

Figure 4: Theorem 4.4 bounds $b(T)$, for $C=\{10,100,1000\}$.

In Figure 4 we present the bound as a function of T for $C=\{10,100,1000\}$. According to the analysis, samples whose Δz is above the bound are those for which the TS operation yields a larger (resp. smaller) prediction set size when $T>1$ (resp. $T<1$). We denote by $T_{critical}$ the temperature value at which the bound attains its minimum value for $T>1$. This value can be computed (numerically) by the intersection of the functions in the max operation at the $T>1$ branch in equation 4.4. Note that it is affected by the number of classes C. Inspecting Figure 4 we gain the following insights.

- For $0<T<1$: The bound increases as a function of T. Thus, as T decreases, a greater proportion of samples satisfy the bound (have $L_T \leq L$), which is aligned with a reduction in the mean prediction set sizes.
- For $1<T<T_{critical}$: The bound decreases as T increases, indicating that more samples comply with the bound (have $L_T \geq L$), which is aligned with an increase in the mean prediction set sizes.

- At $T = T_{critical}$: The bound attains a minimum, corresponding to the maximum number of samples satisfying the bound, which is aligned with the largest mean prediction set size.
- For $T > T_{critical}$: The bound again increases, indicating that as T continues to rise, fewer samples satisfy the bound, which is aligned with a decrease in the prediction set sizes.

We see that $T_{critical}$ describes the temperature at which the trend of the prediction set size shifts from increasing to decreasing as T increases. Our theory shows that $T_{critical}$ shifts to lower temperatures as C increases. A similar trend is observed in the empirical results shown in Figure 2. Specifically, for ImageNet-ViT ($C = 1000$), the empirical maximum of the mean prediction set size occurs at $T = 1.802$, while the bound's minimum is at $T = 1.778$. For CIFAR100-DenseNet121, the empirical maximum is at $T = 2.317$ and the bound's minimum at $T = 2.120$. For CIFAR10-ResNet50, the empirical maximum is at $T = 3.404$, and the bound's minimum at $T = 3.289$. The temperature values derived from our theoretical bounds closely match the empirical results, indicating that our theory effectively captures the impact of the number of classes on the observed behavior.

5 Guidelines for Practitioners

Based on our theoretically-backed findings, we propose a guideline, depicted in Fig. 5, for practitioners that wish to use adaptive CP methods (e.g., due to their better conditional coverage).

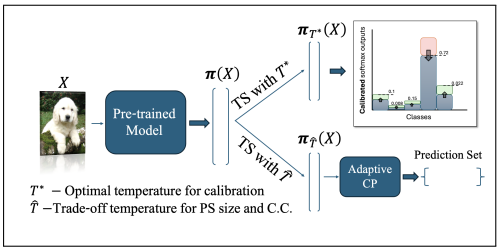

Figure 5: Guideline for using TS calibration and adaptive CP.

Specifically, we suggest to use TS with two different temperature parameters on separate branches: T^* that is optimized for TS calibration, and $\hat{T}$ that allows trading the prediction set sizes and conditional coverage properties of APS/RAPS to better fit the task's requirements. Our experiments and theory show that $\hat{T}$ should be scanned up to a value $T_{critical}$, which can be approximated by our theory (approximately 2 for ImageNet and CIFAR-100).

A limitation is that one does not know in advance what values of the metrics are obtained per value of $\hat{T}$. However, since we propose to separate the calibration and the CP procedure, the calibration set can also be used to evaluate the CP algorithms *without dangering exchangeability*. Indeed, in Appendix C, we demonstrate how using a small amount of calibration data we can approximate the curves of AvgSize and TopCovGap vs. T that appear in Figure 2 (which were generated using the entire validation set that is not accessible to the user in practice). According to the approximate trends, the user can choose $\hat{T}$ that best fit their requirements. Furthermore, note that the procedure required to produce approximated curves of metrics vs. T is done offline during the calibration phase and its runtime is negligible compared to the offline training of DNNs.

In Appendix D, we further show the practical significance of our guidelines. Specifically, for users that prioritize class-conditional coverage, we show that applying TS with $T_{critical}$ followed by RAPS outperforms Mondrian CP (Vovk, 2012) (a method that is based on classwise CP) in both TopCovGap and AvgSize in our CIFAR-100 and ImageNet settings.

6 Conclusion

In this work, we studied the effect of the widely used temperature scaling (TS) calibration on the performance of conformal prediction (CP) techniques. These popular complementary approaches are useful for assessing the reliability of classifiers, in particular those that are based DNNs. Yet, their interplay has not been examined so far. We conducted an extensive empirical study on the effect of TS, even beyond its calibration application, on prominent CP methods. Among our findings, we discovered that TS enables trading prediction set size and class-conditional coverage performance of adaptive CP methods (APS and RAPS) through a non-monotonic pattern, which is similar across all models and datasets examined. We presented a theoretical analysis on the effect of TS on the prediction set sizes of APS and RAPS, which offers a comprehensive explanation for this pattern. Finally, based on our findings, we provided practical guidelines for combining APS and RAPS with calibration while adjusting them via a dedicated TS mechanism to better fit specific requirements. As in this paper we focused on classification, we believe that investigation of the interplay between calibration and CP in regression is an interesting direction for future research.

REPRODUCIBILITY

Please refer to Sections 3.1, 3.3 , B.1 for all the necessary information for reproducing the results.

REFERENCES

Anastasios N Angelopoulos and Stephen Bates. A gentle introduction to conformal prediction and distribution-free uncertainty quantification. *arXiv preprint arXiv:2107.07511*, 2021.

Anastasios Nikolas Angelopoulos, Stephen Bates, Michael Jordan, and Jitendra Malik. Uncertainty sets for image classifiers using conformal prediction. In *International Conference on Learning Representations*, 2021.

Rina Foygel Barber, Emmanuel J Candes, Aaditya Ramdas, and Ryan J Tibshirani. Conformal prediction beyond exchangeability. *The Annals of Statistics*, 51(2):816–845, 2023.

Leda Cosmides and John Tooby. Are humans good intuitive statisticians after all? rethinking some conclusions from the literature on judgment under uncertainty. *cognition*, 58(1):1–73, 1996.

Morris H DeGroot and Stephen E Fienberg. The comparison and evaluation of forecasters. *Journal of the Royal Statistical Society: Series D (The Statistician)*, 32(1-2):12–22, 1983.

Jia Deng, Wei Dong, Richard Socher, Li-Jia Li, Kai Li, and Li Fei-Fei. Imagenet: A large-scale hierarchical image database. In *2009 IEEE conference on computer vision and pattern recognition*, pp. 248–255. Ieee, 2009.

Tiffany Ding, Anastasios Angelopoulos, Stephen Bates, Michael Jordan, and Ryan J Tibshirani. Class-conditional conformal prediction with many classes. *Advances in Neural Information Processing Systems*, 36, 2023.

Zhipeng Ding, Xu Han, Peirong Liu, and Marc Niethammer. Local temperature scaling for probability calibration. In *Proceedings of the IEEE/CVF International Conference on Computer Vision*, pp. 6889–6899, 2021.

Alexey Dosovitskiy, Lucas Beyer, Alexander Kolesnikov, Dirk Weissenborn, Xiaohua Zhai, Thomas Unterthiner, Mostafa Dehghani, Matthias Minderer, Georg Heigold, Sylvain Gelly, Jakob Uszkoreit, and Neil Houlsby. An image is worth 16x16 words: Transformers for image recognition at scale. In *International Conference on Learning Representations*, 2021.

Rina Foygel Barber, Emmanuel J Candes, Aaditya Ramdas, and Ryan J Tibshirani. The limits of distribution-free conditional predictive inference. *Information and Inference: A Journal of the IMA*, 10(2):455–482, 2021.

Lior Frenkel and Jacob Goldberger. Network calibration by class-based temperature scaling. In *2021 29th European Signal Processing Conference (EUSIPCO)*, pp. 1486–1490. IEEE, 2021.

Isaac Gibbs, John J Cherian, and Emmanuel J Candès. Conformal prediction with conditional guarantees. *arXiv preprint arXiv:2305.12616*, 2023.

Sorin Grigorescu, Bogdan Trasnea, Tiberiu Cocias, and Gigel Macesanu. A survey of deep learning techniques for autonomous driving. *Journal of Field Robotics*, 37(3):362–386, 2020.

Chuan Guo, Geoff Pleiss, Yu Sun, and Kilian Q Weinberger. On calibration of modern neural networks. In *International conference on machine learning*, pp. 1321–1330. PMLR, 2017.

Wenbo Guo, Dongliang Mu, Jun Xu, Purui Su, Gang Wang, and Xinyu Xing. Lemna: Explaining deep learning based security applications. In *proceedings of the 2018 ACM SIGSAC conference on computer and communications security*, pp. 364–379, 2018.

Trevor Hastie, Robert Tibshirani, Jerome Friedman, and James Franklin. The elements of statistical learning: data mining, inference and prediction. *The Mathematical Intelligencer*, 27(2):83–85, 2005.

Kaiming He, Xiangyu Zhang, Shaoqing Ren, and Jian Sun. Deep residual learning for image recognition. In *Proceedings of the IEEE conference on computer vision and pattern recognition*, pp. 770–778, 2016.

Gao Huang, Zhuang Liu, Laurens Van Der Maaten, and Kilian Q Weinberger. Densely connected convolutional networks. In *Proceedings of the IEEE conference on computer vision and pattern recognition*, pp. 4700–4708, 2017.

Byeongmoon Ji, Hyemin Jung, Jihyeun Yoon, Kyungyul Kim, et al. Bin-wise temperature scaling (bts): Improvement in confidence calibration performance through simple scaling techniques. In *2019 IEEE/CVF International Conference on Computer Vision Workshop (ICCVW)*, pp. 4190–4196. IEEE, 2019.

Alex Krizhevsky, Geoffrey Hinton, et al. Learning multiple layers of features from tiny images. 2009.

Alex Krizhevsky, Ilya Sutskever, and Geoffrey E Hinton. Imagenet classification with deep convolutional neural networks. *Advances in neural information processing systems*, 25, 2012.

Jing Lei and Larry Wasserman. Distribution-free prediction bands for non-parametric regression. *Journal of the Royal Statistical Society Series B: Statistical Methodology*, 76(1):71–96, 2014.

Shiyu Liang, Yixuan Li, and R Srikant. Enhancing the reliability of out-of-distribution image detection in neural networks. In *International Conference on Learning Representations*, 2018.

Charles Lu, Syed Rakin Ahmed, Praveer Singh, and Jayashree Kalpathy-Cramer. Estimating test performance for ai medical devices under distribution shift with conformal prediction. *arXiv preprint arXiv:2207.05796*, 2022.

Charles Lu, Yaodong Yu, Sai Praneeth Karimireddy, Michael Jordan, and Ramesh Raskar. Federated conformal predictors for distributed uncertainty quantification. In *International Conference on Machine Learning*, pp. 22942–22964. PMLR, 2023.

Riccardo Miotto, Fei Wang, Shuang Wang, Xiaoqian Jiang, and Joel T Dudley. Deep learning for healthcare: review, opportunities and challenges. *Briefings in bioinformatics*, 19(6):1236–1246, 2018.

Mahdi Pakdaman Naeini, Gregory Cooper, and Milos Hauskrecht. Obtaining well calibrated probabilities using bayesian binning. In *Proceedings of the AAAI conference on artificial intelligence*, volume 29, 2015.

Alexandru Niculescu-Mizil and Rich Caruana. Predicting good probabilities with supervised learning. In *Proceedings of the 22nd international conference on Machine learning*, pp. 625–632, 2005.

Jeremy Nixon, Michael W Dusenberry, Linchuan Zhang, Ghassen Jerfel, and Dustin Tran. Measuring calibration in deep learning. In *CVPR workshops*, volume 2, 2019.

Harris Papadopoulos, Kostas Proedrou, Volodya Vovk, and Alex Gammerman. Inductive confidence machines for regression. In *Machine Learning: ECML 2002: 13th European Conference on Machine Learning Helsinki, Finland, August 19–23, 2002 Proceedings 13*, pp. 345–356. Springer, 2002.

John Platt et al. Probabilistic outputs for support vector machines and comparisons to regularized likelihood methods. *Advances in large margin classifiers*, 10(3):61–74, 1999.

Yaniv Romano, Matteo Sesia, and Emmanuel Candes. Classification with valid and adaptive coverage. *Advances in Neural Information Processing Systems*, 33:3581–3591, 2020.

Mauricio Sadinle, Jing Lei, and Larry Wasserman. Least ambiguous set-valued classifiers with bounded error levels. *Journal of the American Statistical Association*, 114(525):223–234, 2019.

David Stutz, Ali Taylan Cemgil, Arnaud Doucet, et al. Learning optimal conformal classifiers. In *International Conference on Learning Representations*, 2022.

Ryan J Tibshirani, Rina Foygel Barber, Emmanuel Candes, and Aaditya Ramdas. Conformal prediction under covariate shift. *Advances in neural information processing systems*, 32, 2019.

Vladimir Vovk. Conditional validity of inductive conformal predictors. In *Asian conference on machine learning*, pp. 475–490. PMLR, 2012.

Vladimir Vovk, Alexander Gammerman, and Glenn Shafer. *Algorithmic learning in a random world*, volume 29. Springer, 2005.

Volodya Vovk, Alexander Gammerman, and Craig Saunders. Machine-learning applications of algorithmic randomness. In *Proceedings of the Sixteenth International Conference on Machine Learning*, pp. 444–453, 1999.

Deng-Bao Wang, Lei Feng, and Min-Ling Zhang. Rethinking calibration of deep neural networks: Do not be afraid of overconfidence. *Advances in Neural Information Processing Systems*, 34: 11809–11820, 2021.

Hongxin Wei, Renchunzi Xie, Hao Cheng, Lei Feng, Bo An, and Yixuan Li. Mitigating neural network overconfidence with logit normalization. In *International Conference on Machine Learning*, pp. 23631–23644. PMLR, 2022.

Bianca Zadrozny and Charles Elkan. Transforming classifier scores into accurate multiclass probability estimates. In *Proceedings of the eighth ACM SIGKDD international conference on Knowledge discovery and data mining*, pp. 694–699, 2002.

A PROOFS.

Theorem A.1. *Let $\mathbf{z} \in \mathbb{R}^C$ be a sorted logits vector, i.e., $z_1 \geq z_2 \geq \ldots \geq z_C$, and let $L \in [C]$. Let $\hat{\boldsymbol{\pi}}_T = \boldsymbol{\sigma}(\mathbf{z}/T)$ and $\hat{\boldsymbol{\pi}}_{\tilde{T}} = \boldsymbol{\sigma}(\mathbf{z}/\tilde{T})$ with $T > \tilde{T} > 0$. Then, we have $\sum_{j=1}^{L} \pi_{\tilde{T},j} \geq \sum_{j=1}^{L} \pi_{T,j}$. The inequality is strict, unless $L = C$ or $z_1 = \ldots = z_C$.*

Before we turn to prove the theorem, let us prove an auxiliary lemma.

Lemma. *Let $z_i, z_j \in \mathbb{R}$ such that $z_i \geq z_j$ and let $T \geq \tilde{T} \geq 0$. Then, the following holds*

$$\exp(z_i/\tilde{T}) \cdot \exp(z_j/T) \geq \exp(z_i/T) \cdot \exp(z_j/\tilde{T}).$$

The inequality is strict, unless $T = \tilde{T}$ or $z_i = z_j$.

Proof. Since $z_i - z_j \geq 0$ and $\tilde{T} - \tilde{T}/T \geq 0$ we have that

$$\exp\left[(z_i - z_j)\left(\tilde{T} - \frac{\tilde{T}}{T}\right)\right] \geq 1,$$

where the inequality is strict, unless $T = \tilde{T}$ or $z_i = z_j$. Next, observe that

$$\begin{aligned}
\exp\left[(z_i - z_j)\left(\tilde{T} - \frac{\tilde{T}}{T}\right)\right] &= \exp\left[z_i\left(\tilde{T} - \frac{\tilde{T}}{T}\right) - z_j\left(\tilde{T} - \frac{\tilde{T}}{T}\right)\right] \\
&= \frac{\exp\left(\frac{z_i}{\tilde{T}} + \frac{z_j}{T}\right)}{\exp\left(\frac{z_i}{T} + \frac{z_j}{\tilde{T}}\right)} \\
&= \frac{\exp(z_i/\tilde{T}) \cdot \exp(z_j/T)}{\exp(z_i/T) \cdot \exp(z_j/\tilde{T})}.
\end{aligned}$$

Using the inequality we have $\dfrac{\exp(z_i/\tilde{T}) \cdot \exp(z_j/T)}{\exp(z_i/T) \cdot \exp(z_j/\tilde{T})} \geq 1$, which concludes the proof of the lemma. □

Proof. **Back to the proof of the theorem.**

Let $I = \{1, 2, \ldots, L\}$ and $J = \{L+1, L+2, \ldots, C\}$. Because $\mathbf{z}$ is sorted, $\forall i \in I, j \in J$ we have $z_i > z_j$. Therefore, according to the auxiliary lemma in Theorem A.1: $\exp(z_i/\tilde{T}) \cdot \exp(z_j/T) \geq \exp(z_i/T) \cdot \exp(z_j/\tilde{T})$ for any combination of $i \in I, j \in J$. Consequently, summing this inequality over all $i \in I, j \in J$, we get

$$\begin{aligned}
&\sum_{i=1}^{L} \sum_{j=L+1}^{C} \exp(z_i/\tilde{T}) \cdot \exp(z_j/T) \geq \sum_{i=1}^{L} \sum_{j=L+1}^{C} \exp(z_i/T) \cdot \exp(z_j/\tilde{T}) \\
&\qquad\qquad \Updownarrow \\
&\sum_{i=1}^{L} \exp(z_i/\tilde{T}) \cdot \sum_{j=L+1}^{C} \exp(z_j/T) \geq \sum_{i=1}^{L} \exp(z_i/T) \cdot \sum_{j=L+1}^{C} \exp(z_j/\tilde{T}).
\end{aligned}$$

In the last line, we separated the summation of the indexes $i \in I, j \in J$.

Adding $\sum_{i=1}^{L}\exp(z_i/\tilde{T})\cdot\sum_{j=1}^{L}\exp(z_j/T)$ to both sides, we get

$$\sum_{i=1}^{L}\exp(z_i/\tilde{T})\left[\sum_{i=1}^{L}\exp\left(z_i/T\right)+\sum_{j=L+1}^{C}\exp\left(z_j/T\right)\right]\geq\sum_{j=1}^{L}\exp\left(z_j/T\right)\left[\sum_{i=1}^{L}\exp(z_i/\tilde{T})+\sum_{j=L+1}^{C}\exp(z_j/\tilde{T})\right]$$

$$\Updownarrow$$

$$\sum_{i=1}^{L}\exp(z_i/\tilde{T})\sum_{j=1}^{C}\exp\left(z_j/T\right)\geq\sum_{i=1}^{L}\exp\left(z_i/T\right)\sum_{j=1}^{C}\exp(z_j/\tilde{T})$$

$$\Updownarrow$$

$$\frac{\sum_{i=1}^{L}\exp(z_i/\tilde{T})}{\sum_{j=1}^{C}\exp(z_j/\tilde{T})}\geq\frac{\sum_{i=1}^{L}\exp\left(z_i/T\right)}{\sum_{j=1}^{C}\exp\left(z_j/T\right)}$$

$$\Updownarrow$$

$$\sum_{j=1}^{L}\frac{\exp(z_j/\tilde{T})}{\sum_{c=1}^{C}\exp\left(z_c/\tilde{T}\right)}\geq\sum_{j=1}^{L}\frac{\exp(z_j/T)}{\sum_{c=1}^{C}\exp\left(z_c/T\right)}$$

as stated in the theorem. Note that the inequality is strict unless $L=C$ (both sides equal 1) or $T=\tilde{T}$ or $z_1=\ldots=z_C$ (all the pairs are equal).

□

Corollary A.2. *The threshold value $\hat{q}_T$ of APS and RAPS decreases monotonically as the temperature T increases.*

Proof. Let us start with APS. Set $T\geq\tilde{T}$. For each sample $(\mathbf{x},y)$ in the CP set, we get the post softmax vectors $\hat{\boldsymbol{\pi}}_T$ and $\hat{\boldsymbol{\pi}}$, with and without TS, respectively. By Theorem 4.1, applied on the sorted vector $\boldsymbol{\pi}=[\hat{\pi}_{(1)},\ldots,\hat{\pi}_{(C)}]^\top$ with $L=L_y$ (the index that y is permuted to after sorting), we have that

$$\sum\nolimits_{j=1}^{L_y}\pi_{\tilde{T},j}\geq\sum\nolimits_{j=1}^{L_y}\pi_{T,j}\tag{7}$$

That is, the score of APS decreases *universally* for each sample in the CP set. This implies that $\hat{q}$, the $\frac{\lceil(n+1)(1-\alpha)\rceil}{n}$ quantile of the scores of the samples of the CP set, decreases as well.

We turn to consider RAPS. In this case, a decrease due to TS in the score of each sample $(\mathbf{x},y)$ in the CP set, i.e.,

$$\sum_{i=1}^{L_y}\hat{\pi}_{\tilde{T},(i)}(\mathbf{x})+\lambda(L_y-k_{reg})_+\geq\sum_{i=1}^{L_y}\hat{\pi}_{T,(i)}(\mathbf{x})+\lambda(L_y-k_{reg})_+,$$

simply follows from adding $\lambda(L_y-k_{reg})_+$ to both sides of equation 7. The rest of the arguments are exactly as in APS.

□

Proposition A.3. *Let $\mathbf{z}\in\mathbb{R}^C$ such that $z_1\geq z_2\geq\cdots\geq z_C$, $\hat{\boldsymbol{\pi}}_T=\boldsymbol{\sigma}(\mathbf{z}/T)$ and $\hat{\boldsymbol{\pi}}=\boldsymbol{\sigma}(\mathbf{z})$. Let $\hat{q},\hat{q}_T\in(0,1]$ such that if $T>1$ then $\hat{q}\geq\hat{q}_T$ and if $0<T<1$ then $\hat{q}\leq\hat{q}_T$. Let $L=\min\{l:\sum_{i=1}^{l}\hat{\pi}_i\geq\hat{q}\}$, $L_T=\min\{l:\sum_{i=1}^{l}\hat{\pi}_{T,i}\geq\hat{q}_T\}$. The following holds:*

$$\begin{cases}\textit{If}\quad 0<T<1,\quad \textit{then}:\quad \forall M\in[L]:\quad \sum_{i=1}^{M}\hat{\pi}_i-\sum_{i=1}^{M}\hat{\pi}_{T,i}\leq\hat{q}-\hat{q}_T\implies L\geq L_T\\ \textit{If}\quad T>1,\quad \textit{then}:\quad \forall M\in[L]:\quad \sum_{i=1}^{M}\hat{\pi}_i-\sum_{i=1}^{M}\hat{\pi}_{T,i}\geq\hat{q}-\hat{q}_T\implies L\leq L_T\end{cases}\tag{8}$$

Proof. We start with **T > 1 branch:** for which $\hat{q} \geq \hat{q}_T$:

$$\forall M \in [L]: \quad \sum_{i=1}^{M} \hat{\pi}_i - \sum_{i=1}^{M} \hat{\pi}_{T,i} \geq \hat{q} - \hat{q}_T \iff \forall M \in [L]: \quad \sum_{i=1}^{M} \hat{\pi}_i \geq \hat{q} - \hat{q}_T + \sum_{i=1}^{M} \hat{\pi}_{T,i}$$

Note that for every $0 < x \leq \hat{q}$ we have $M_x := \min\{l : \sum_{i=1}^{l} \hat{\pi}_i \geq x\} \leq L$. For $M_x > 1$ (i.e., not minimal possible value), the event implies $\hat{q} - \hat{q}_T + \sum_{i=1}^{M_x-1} \hat{\pi}_{T,i} \leq \sum_{i=1}^{M_x-1} \hat{\pi}_i < x$. This implies that $\min\{l : \hat{q} - \hat{q}_T + \sum_{i=1}^{l} \hat{\pi}_{T,i} \geq x\}$ cannot be smaller than M_x. This also trivially holds for $M_x = 1$ (the minimal set size). That is,

$$\implies \forall\ 0 < x \leq \hat{q}: \quad \min\{l : \sum_{i=1}^{l} \hat{\pi}_i \geq x\} \leq \min\{l : \hat{q} - \hat{q}_T + \sum_{i=1}^{l} \hat{\pi}_{T,i} \geq x\}$$

Let us pick $x = \hat{q}$:

$$\min\{l : \sum_{i=1}^{l} \hat{\pi}_i \geq \hat{q}\} \leq \min\{l : \hat{q} - \hat{q}_T + \sum_{i=1}^{l} \hat{\pi}_{T,i} \geq \hat{q}\}$$

$$\iff \min\{l : \sum_{i=1}^{l} \hat{\pi}_i \geq \hat{q}\} \leq \min\{l : \sum_{i=1}^{l} \hat{\pi}_{T,i} \geq \hat{q}_T\} \iff L \leq L_T$$

We continue with **0 < T < 1 branch:**, for which $\hat{q}_T \geq \hat{q}$, we will take similar steps:

$$\forall M \in [L]: \quad \sum_{i=1}^{M} \hat{\pi}_i - \sum_{i=1}^{M} \hat{\pi}_{T,i} \leq \hat{q} - \hat{q}_T \iff \forall M \in [L]: \quad \sum_{i=1}^{M} \hat{\pi}_{T,i} \geq \hat{q}_T - \hat{q} + \sum_{i=1}^{M} \hat{\pi}_i$$

Note that for every $0 < x \leq \hat{q}_T$ we have $M_x := \min\{l : \sum_{i=1}^{l} \hat{\pi}_{i,T} \geq x\} \leq L$. For $M_x > 1$ (i.e., not minimal possible value), the event implies $\hat{q}_T - \hat{q} + \sum_{i=1}^{M_x-1} \hat{\pi}_i \leq \sum_{i=1}^{M_x-1} \hat{\pi}_{i,T} < x$. This implies that $\min\{l : \hat{q}_T - \hat{q} + \sum_{i=1}^{M_x-1} \hat{\pi}_i \geq x\}$ cannot be smaller than M_x. That is,

$$\implies \forall\ 0 < x \leq \hat{q}_T: \quad \min\{l : \sum_{i=1}^{l} \hat{\pi}_{i,T} \geq x\} \leq \min\{l : \hat{q}_T - \hat{q} + \sum_{i=1}^{M_x-1} \hat{\pi}_i \geq x\}$$

Let us pick $x = \hat{q}_T$:

$$\min\{l : \sum_{i=1}^{l} \hat{\pi}_{i,T} \geq \hat{q}_T\} \leq \min\{l : \hat{q}_T - \hat{q} + \sum_{i=1}^{M_x-1} \hat{\pi}_i \geq \hat{q}_T\}$$

$$\iff \min\{l : \sum_{i=1}^{l} \hat{\pi}_{i,T} \geq \hat{q}_T\} \leq \min\{l : \sum_{i=1}^{M_x-1} \hat{\pi}_i \geq \hat{q}\} \iff L_T \leq L$$

□

Theorem A.4. *Let* $\mathbf{z} \in \mathbb{R}^C$ *such that* $z_1 \geq z_2 \geq \cdots \geq z_C$ *and denote* $\Delta z = z_1 - z_2$. *Then, the following holds:*

$$\begin{cases} \textit{If} \quad 0 < T < 1: \quad \Delta z > \max\left\{ \dfrac{T}{T-1} \ln\left(\dfrac{T}{4}\right), \dfrac{T}{T+1} \ln\left(\dfrac{4(C-1)^2}{T}\right) \right\} \implies \nabla_{z_1} g(\mathbf{z}; T, M) > 0 \\ \textit{If} \quad T > 1: \quad \Delta z > \max\left\{ \dfrac{T}{T-1} \ln(4T), \dfrac{T-1}{T+1} \ln(4T(C-1)^2) \right\} \implies \nabla_{z_1} g(\mathbf{z}; T, M) < 0 \end{cases} \tag{9}$$

Proof. Let us start with **T > 1 branch:** The gap function is defined as follows:

$$g_z(\mathbf{z}; T, M) = \frac{\sum_{i=1}^{M} \exp(z_i)}{\sum_{j=1}^{C} \exp(z_j)} - \frac{\sum_{i=1}^{M} \exp(z_i/T)}{\sum_{j=1}^{C} \exp(z_j/T)}$$

Let us differentiate with respect to z_1

$$\begin{aligned} \nabla_{z_1} g_z(\mathbf{z}; T, M) &= \frac{\exp(z_1)\left[\sum_{j=1}^{C} \exp(z_j) - \sum_{i=1}^{M} \exp(z_i)\right]}{\left[\sum_{j=1}^{C} \exp(z_j)\right]^2} - \frac{\frac{1}{T}\exp(z_1/T)\left[\sum_{j=1}^{C} \exp(z_j/T) - \sum_{i=1}^{M} \exp(z_i/T)\right]}{\left[\sum_{j=1}^{C} \exp(z_j/T)\right]^2} \\ &= \frac{\exp(z_1)\sum_{c=M+1}^{C} \exp(z_c)}{\left[\sum_{c=1}^{C} \exp(z_c)\right]^2} - \frac{\frac{1}{T}\exp(z_1/T)\sum_{c=M+1}^{C} \exp(z_c/T)}{\left[\sum_{c=1}^{C} \exp(z_c/T)\right]^2} \end{aligned}$$

Therefore,

$$\nabla_{z_1} g_z(\mathbf{z}; T, M) < 0 \iff \exp\left(z_1\left(1 - \frac{1}{T}\right)\right) < \frac{1}{T}\frac{\sum_{c=M+1}^{C} \exp(z_c/T)}{\sum_{c=M+1}^{C} \exp(z_c)} \left[\frac{\sum_{c=1}^{C} \exp(z_c)}{\sum_{c=1}^{C} \exp(z_c/T)}\right]^2 \tag{10}$$

where we arranged the inequality and used $\exp(z_1)/\exp(z_1/T) = \exp\left(z_1\left(1 - \frac{1}{T}\right)\right)$.

According to the auxiliary lemma in Theorem A.1, if we substitute $\tilde{T} = 1$ we get: for all $z_i > z_j$ and $T > 1$ we have $\exp(z_i) \cdot \exp(z_j/T) > \exp(z_i/T) \cdot \exp(z_j)$.

Therefore, taking $i = M+1$ and summing both sides of the inequality over $j = M+1, ..., C$, the following holds:

$$\frac{\sum_{c=M+1}^{C} \exp(z_c/T)}{\sum_{c=M+1}^{C} \exp(z_c)} > \frac{\exp(z_{M+1}/T)}{\exp(z_{M+1})} \tag{11}$$

In addition, note that $\forall A$ such that $A > \max\left(2(C-1)\exp(-\Delta z/T), 2\right)$ we get:

$$A > (C-1)\exp(-\Delta z/T) + 1 \implies A\exp(z_1/T) > \sum_{c=1}^{C} \exp(z_c/T) \tag{12}$$

where the implication follows from

$$\sum_{c=1}^{C} \exp(z_c/T)/\exp(z_1/T) = 1 + \sum_{c=2}^{C} \exp(-(z_1 - z_c)/T) \leq 1 + (C-1)\exp(-(z_1 - z_2)/T).$$

Using the above inequalities (equation 11 and equation 12) we obtain

$$\frac{1}{T}\frac{\sum_{c=M+1}^{C} \exp(z_c/T)}{\sum_{c=M+1}^{C} \exp(z_c)} \left[\frac{\sum_{c=1}^{C} \exp(z_c)}{\sum_{c=1}^{C} \exp(z_c/T)}\right]^2 > \frac{1}{T}\frac{\exp(z_{M+1}/T)}{\exp(z_{M+1})} \left[\frac{\exp(z_1)}{A\exp(z_1/T)}\right]^2 \geq \frac{1}{A^2 T}\exp\left((2z_1 - z_2)\left(1 - \frac{1}{T}\right)\right)$$

where in the last inequality we used

$$\frac{\exp(z_{M+1}/T)}{\exp(z_{M+1})}\frac{\exp(z_1)}{\exp(z_1/T)} = \exp\left((z_1 - z_{M+1})\left(1-\frac{1}{T}\right)\right) \geq \exp\left((z_1 - z_2)\left(1-\frac{1}{T}\right)\right).$$

Hence, according to equation 10: $\exp\left(z_1\left(1-\frac{1}{T}\right)\right) < \frac{1}{A^2T}\exp\left((2z_1 - z_2)\left(1-\frac{1}{T}\right)\right) \implies \nabla_{z_1} g_z(\mathbf{z}; T, M) < 0$

Note that

$$\exp\left(z_1\left(1-\frac{1}{T}\right)\right) < \frac{1}{A^2T}\exp\left((2z_1 - z_2)\left(1-\frac{1}{T}\right)\right)$$
$$\iff 1 < \frac{1}{A^2T}\exp\left((z_1 - z_2)\left(1-\frac{1}{T}\right)\right) \iff \Delta z > \frac{T}{T-1}\ln(A^2T)$$

And by using the definition of A we obtain:

$$\Delta z > \max\left(\frac{T}{T-1}\ln(4T), \frac{T-1}{T+1}\ln(4T(C-1)^2)\right) \implies \nabla_{z_1} g_z(\mathbf{z}; T, M) < 0$$

We continue with **0 < T < 1 branch:** Based on steps we took for the previous branch:

$$\nabla_{z_1} g_z(\mathbf{z}; T, M) > 0 \iff \exp\left(z_1\left(1-\frac{1}{T}\right)\right) > \frac{1}{T}\frac{\sum_{c=M+1}^{C}\exp(z_c/T)}{\sum_{c=M+1}^{C}\exp(z_c)}\left[\frac{\sum_{c=1}^{C}\exp(z_c)}{\sum_{c=1}^{C}\exp(z_c/T)}\right]^2 \tag{13}$$

Note that according to the auxiliary lemma in Theorem A.1, if we substitute $\tilde{T} = 1$ we get: for all $z_i > z_j$ and $0 < T < 1$ we have $\exp(z_i)\cdot\exp(z_j/T) > \exp(z_i/T)\cdot\exp(z_j)$ and therefore the following holds:

$$\frac{\sum_{c=M+1}^{C}\exp(z_c)}{\sum_{c=M+1}^{C}\exp(z_c/T)} > \frac{\exp(z_{M+1})}{\exp(z_{M+1}/T)}$$

In addition, note that $\forall A$ such that $A > \max\left(2(C-1)\exp(-\Delta z), 2\right)$ we get:

$$A > (C-1)\exp(-\Delta z) + 1 \implies A\exp(z_1) > \sum_{c=1}^{C}\exp(z_c) \tag{14}$$

Using above inequalities we obtain

$$\frac{1}{T}\frac{\sum_{c=M+1}^{C}\exp(z_c/T)}{\sum_{c=M+1}^{C}\exp(z_c)}\left[\frac{\sum_{c=1}^{C}\exp(z_c)}{\sum_{c=1}^{C}\exp(z_c/T)}\right]^2 < \frac{1}{T}\frac{\exp(z_{M+1}/T)}{\exp(z_{M+1})}\left[\frac{A\exp(z_1)}{\exp(z_1/T)}\right]^2 \leq \frac{A^2}{T}\exp\left((2z_1 - z_2)\left(1-\frac{1}{T}\right)\right)$$

Hence, according to equation 13: $\exp\left(z_1\left(1-\frac{1}{T}\right)\right) > \frac{A^2}{T}\exp\left((2z_1 - z_2)\left(1-\frac{1}{T}\right)\right) \implies \nabla_{z_1} g_z(\mathbf{z}; T, M) > 0$

Note that

$$\exp\left(z_1\left(1-\frac{1}{T}\right)\right) > \frac{A^2}{T}\exp\left((2z_1 - z_2)\left(1-\frac{1}{T}\right)\right) \iff \Delta z > \frac{T}{T-1}\ln\left(\frac{T}{A^2}\right)$$

The sign of the in-equality changed because $1 - \frac{1}{T} < 0$.

And by using the definition of A we obtain:

$$\Delta z > \max\left(\frac{T}{T-1}\ln\left(\frac{T}{4}\right), \frac{T-1}{T+1}\ln\left(\frac{4(C-1)^2}{T}\right)\right) \implies \nabla_{z_1} g_z(\mathbf{z}; T, M) > 0$$

□

Proposition A.5. *Let $\mathbf{z} \in \mathbb{R}^C$, $\boldsymbol{\sigma}(\cdot)$ be the softmax function, and Δ^{C-1} denote the simplex in $\mathbb{R}^C$. Consider Shannon's entropy $H : \Delta^{C-1} \to \mathbb{R}$, i.e., $H(\boldsymbol{\pi}) = -\sum_{i=1}^{C} \pi_i \ln(\pi_i)$. Unless $\mathbf{z} \propto \mathbf{1}_C$ (then $\boldsymbol{\sigma}(\mathbf{z}/T) = \boldsymbol{\sigma}(\mathbf{z})$), we have that $H(\boldsymbol{\sigma}(\mathbf{z}/T))$ is strictly monotonically increasing as T grows.*

Proof. To prove this statement, let us show that the function $f(T) = H(\boldsymbol{\sigma}(\mathbf{z}/T))$ monotonically increases (as T increases, regardless of $\mathbf{z}$). To achieve this, we need to show that $f'(T) = \frac{d}{dT} H(\boldsymbol{\sigma}(\mathbf{z}/T)) \geq 0$.

By the chain-rule, $f'(T) = \frac{d}{dT}\left(H(\boldsymbol{\sigma}(\mathbf{z}/T))\right) = \frac{\partial H(\boldsymbol{\sigma})}{\partial \boldsymbol{\sigma}} \frac{\partial \boldsymbol{\sigma}(\mathbf{z})}{\partial \mathbf{z}} \frac{\partial}{\partial T}(\mathbf{z}/T)$. Let us compute each term:

$$\frac{\partial H(\boldsymbol{\sigma})}{\partial \sigma_i} = -\ln(\sigma_i) - \frac{1}{\sigma_i} \cdot \sigma_i = -\ln(\sigma_i) - 1 \implies \frac{\partial H(\boldsymbol{\sigma})}{\partial \boldsymbol{\sigma}} = -\ln(\boldsymbol{\sigma})^\top - \mathbf{1}_C^\top$$

$$\frac{\partial \sigma_i(\mathbf{z})}{\partial z_j} = \sigma_i(\mathbf{z}) \cdot (\mathbb{1}\{i=j\} - \sigma_j(\mathbf{z})) \implies \frac{\partial \boldsymbol{\sigma}(\mathbf{z})}{\partial \mathbf{z}} = \mathrm{diag}(\boldsymbol{\sigma}(\mathbf{z})) - \boldsymbol{\sigma}(\mathbf{z})\boldsymbol{\sigma}(\mathbf{z})^\top$$

$$\frac{\partial}{\partial T}(\mathbf{z}/T) = -\frac{1}{T^2}\mathbf{z}$$

where in $\ln(\boldsymbol{\sigma})$ the function operates entry-wise and $\mathbb{1}\{i=j\}$ is the indicator function (equals 1 if $i=j$ and 0 otherwise).

Next, observe that $\mathbf{1}_C^\top \left(\mathrm{diag}(\boldsymbol{\sigma}) - \boldsymbol{\sigma}\boldsymbol{\sigma}^\top\right) = \boldsymbol{\sigma}^\top - \boldsymbol{\sigma}^\top = \mathbf{0}^\top$. Consequently, we get

$$\begin{aligned}
\frac{d}{dT}\left(H(\boldsymbol{\sigma}(\mathbf{z}/T))\right) &= \frac{1}{T^2}\ln(\boldsymbol{\sigma}(\mathbf{z}))^\top(\mathrm{diag}(\boldsymbol{\sigma}(\mathbf{z})) - \boldsymbol{\sigma}(\mathbf{z})\boldsymbol{\sigma}(\mathbf{z})^\top)\mathbf{z} \\
&= \frac{1}{T^2}\left(\mathbf{z} - s(\mathbf{z})\mathbf{1}_C\right)^\top(\mathrm{diag}(\boldsymbol{\sigma}(\mathbf{z})) - \boldsymbol{\sigma}(\mathbf{z})\boldsymbol{\sigma}(\mathbf{z})^\top)\mathbf{z} \\
&= \frac{1}{T^2}\mathbf{z}^\top(\mathrm{diag}(\boldsymbol{\sigma}(\mathbf{z})) - \boldsymbol{\sigma}(\mathbf{z})\boldsymbol{\sigma}(\mathbf{z})^\top)\mathbf{z}
\end{aligned}$$

where in the second equality we used $[\ln(\boldsymbol{\sigma}(\mathbf{z}))]_i = \ln\left(\frac{\exp(z_i)}{\sum_{j=1}^{C}\exp(z_j)}\right) = z_i - s(\mathbf{z})$.

Therefore, for establishing that $\frac{d}{dT}\left(H(\boldsymbol{\sigma}(\mathbf{z}/T))\right) \geq 0$, we can show that $(\mathrm{diag}(\boldsymbol{\sigma}) - \boldsymbol{\sigma}\boldsymbol{\sigma}^\top)$ is a positive semi-definite matrix. Let $\tilde{\sigma}_i = \exp(z_i)$ and notice that $\sigma_i = \frac{\tilde{\sigma}_i}{\sum_{j=1}^{C}\tilde{\sigma}_j}$. Indeed, for any $\mathbf{u} \in \mathbb{R}^C \setminus \{\mathbf{0}\}$ we have that

$$\begin{aligned}
\mathbf{u}^\top(\mathrm{diag}(\boldsymbol{\sigma}) - \boldsymbol{\sigma}\boldsymbol{\sigma}^\top)\mathbf{u} &= \sum_{i=1}^{C} u_i^2\sigma_i - \left(\sum_{i=1}^{C} u_i\sigma_i\right)^2 \\
&= \frac{\sum_{i=1}^{C} u_i^2\tilde{\sigma}_i \cdot \sum_{j=1}^{C}\tilde{\sigma}_j - \left(\sum_{i=1}^{C} u_i\tilde{\sigma}_i\right)^2}{\left(\sum_{j=1}^{C}\tilde{\sigma}_j\right)^2} \\
&\geq 0,
\end{aligned}$$

where the inequality follows from Cauchy–Schwarz inequality: $\sum_{i=1}^{C} u_i \tilde{\sigma}_i = \sum_{i=1}^{C} u_i \sqrt{\tilde{\sigma}_i}\sqrt{\tilde{\sigma}_i} \leq \sqrt{\sum_{i=1}^{C} u_i^2 \tilde{\sigma}_i}\sqrt{\sum_{j=1}^{C} \tilde{\sigma}_j}$.

Cauchy–Schwarz inequality is attained with equality iff $u_i\sqrt{\tilde{\sigma}_i} = c\sqrt{\tilde{\sigma}_i}$ with the same constant c for $i = 1, \ldots, C$, i.e., when $\mathbf{u} = c\mathbf{1}_C$. Recalling that $\frac{d}{dT}\left(H(\boldsymbol{\sigma}(\mathbf{z}/T))\right) = \frac{1}{T^2}\mathbf{z}^\top(\mathrm{diag}(\boldsymbol{\sigma}) - \boldsymbol{\sigma}\boldsymbol{\sigma}^\top)\mathbf{z}$, this implies that $\frac{d}{dT}\left(H(\boldsymbol{\sigma}(\mathbf{z}/T))\right) = 0 \iff z_1 = \ldots = z_C$, and otherwise $\frac{d}{dT}\left(H(\boldsymbol{\sigma}(\mathbf{z}/T))\right) > 0$.

□

A.1 On the link between equation 3 and equation 5

With our assumption that $\hat{q}$ and $\hat{q}_T$ are associated with the same quantile sample $\mathbf{z}^q$, we have that $\hat{q} - \hat{q}_T$ in equation 3 can be written as $g(\mathbf{z}^q; T, L^q)$, where L^q denotes the rank of the true label of $\mathbf{z}^q$. The left-hand side in equation 3 can be written as $g(\mathbf{z}; T, M)$. Thus, it would facilitate the analysis to study the relation between $g(\mathbf{z}; T, M)$ and $g(\mathbf{z}^q; T, M)$, as in equation 5, rather than by $g(\mathbf{z}; T, M)$ and $g(\mathbf{z}^q; T, L^q)$. Since $\Delta z^q = z^q_{(1)} - z^q_{(2)} \gg 1$, we have found both empirically and theoretically that $g(\mathbf{z}^q, T, M) \approx g(\mathbf{z}^q, T, L^q)$, which justifies studying equation 5.

A.1.1 Empirical justification

Here, we demonstrate empirically that the difference $|g(\mathbf{z}^q; T, M) - g(\mathbf{z}^q; T, L^q)|$ is negligible compared to the difference $|g(\mathbf{z}; T, M) - g(\mathbf{z}^q; T, M)|$.

We consider the quantile sample $\mathbf{z}^q$ associated with $1 - \alpha = 0.9$ and L^q as the rank of its true label. Similarly to the analysis in Section 4, we treat a "typical" sample $\mathbf{z}$ as one with the median score, for which L is chosen by the number of sorted softmax entries require for exceeding the score of $\mathbf{z}^q$.

For the CIFAR100-ResNet50 pair we get:

$$\max_{M\in[L],T\in[0.5,5]} |g(\mathbf{z}^q; T, M) - g(\mathbf{z}^q; T, L^q)| = 0.0031,$$
$$\min_{M\in[L],T\in[0.5,5]} |g(\mathbf{z}; T, M) - g(\mathbf{z}^q; T, M)| = 0.0513.$$

For the ImageNet-ViT pair we get:

$$\max_{M\in[L],T\in[0.5,5]} |g(\mathbf{z}^q; T, M) - g(\mathbf{z}^q; T, L^q)| = 0.051,$$
$$\min_{M\in[L],T\in[0.5,5]} |g(\mathbf{z}; T, M) - g(\mathbf{z}^q; T, M)| = 0.2597.$$

The difference $|g(\mathbf{z}^q; T, M) - g(\mathbf{z}^q; T, L^q)|$ is more than an order of magnitude smaller than $|g(\mathbf{z}; T, M) - g(\mathbf{z}^q; T, M)|$. Similar results are obtained for the other pairs as well. This observation reinforces the study of $|g(\mathbf{z}; T, M) - g(\mathbf{z}^q; T, M)|$.

A.1.2 Theoretical Justification

Below, in Proposition A.6 we show that $\forall M, L^q \in [C]$ the difference $|g(\mathbf{z}^q; T, M) - g(\mathbf{z}^q; T, L^q)|$ decays exponentially with Δz^q. As demonstrated in Figure 3, Δz^q of the quantile sample is very high, which indicates the small value of the bound. The proof of the proposition appears in Section A.2.

Proposition A.6. *Let $\mathbf{z} \in \mathbb{R}^C$ such that $z_1 \geq z_2 \geq \cdots \geq z_C$. Consider the following functions:*

$$d(\mathbf{z}; T, i) = \frac{\exp(z_i)}{\sum_{j=1}^{C}\exp(z_j)} - \frac{\exp(z_i/T)}{\sum_{j=1}^{C}\exp(z_j/T)}$$

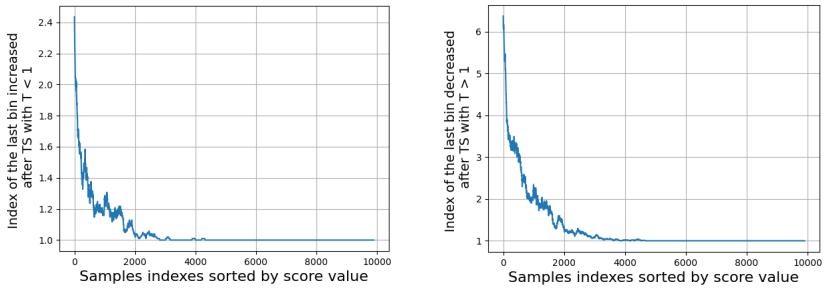

Figure 6: Considering CIFAR100-ResNet50 with sorted logits vectors. Left: the last index increased by TS with $T = 0.5$; Right: the last index decreased by TS with $T = 1.5$, for each sample sorted by score value. We see that $s_{T<1} = 1$ and $s_{T>1} = 1$ for the quantile sample.

$$g(\mathbf{z}; T, M) = \frac{\sum_{i=1}^{M} \exp(z_i)}{\sum_{j=1}^{C} \exp(z_j)} - \frac{\sum_{i=1}^{M} \exp(z_i/T)}{\sum_{j=1}^{C} \exp(z_j/T)} = \sum_{i=1}^{M} d(\mathbf{z}; T, i)$$

Let $s_{T>1} = \max\{i \in [C] : d(\mathbf{z}; T, j) > 0\}$, i.e., the last index where $d(\mathbf{z}, T, \cdot)$ is positive. Similarly, let $s_{T<1} = \max\{i \in [C] : d(\mathbf{z}; T, j) < 0\}$, i.e., the last index where $d(\mathbf{z}, T, \cdot)$ is negative. The following holds:

$$\begin{cases} \textit{If} \quad 0 < T < 1: \quad s_{T<1} = 1 \implies \forall M, L^q \in [C] \quad |g(\mathbf{z}; T, M) - g(\mathbf{z}; T, L^q)| < \dfrac{(C-1)\exp(-\Delta z)}{(C-1)\exp(-\Delta z) + 1} \\ \textit{If} \quad T > 1: \quad s_{T>1} = 1 \implies \forall M, L^q \in [C] \quad |g(\mathbf{z}; T, M) - g(\mathbf{z}; T, L^q)| < \dfrac{(C-1)\exp(-\Delta z/T)}{(C-1)\exp(-\Delta z/T) + 1} \end{cases}$$

When applying the proposition on the quantile sample $\mathbf{z}^q$, since it has $\Delta z^q \gg 1$ we get small upper bounds.

As can be seen in the proposition, the bounds require that $s_{T<1}$ and $s_{T=1}$ equal 1. Recall also that the logits vector is sorted. For $T > 1$ (resp. $T < 1$), this means that the TS attenuates (resp. amplifies) only the maximal softmax bin. This is expected to hold for the quantile sample, due to having a very dominant entry in $\mathbf{z}^q$. We show it empirically in Figure 6, which presents the curves for $s_{T<1}$ and $s_{T>1}$ across samples sorted by their scores for CIFAR100-ResNet50. Both curves indicate that approximately the first third of the samples correspond to $s > 1$, while higher-score samples align with $s = 1$. Notably, for the quantile sample $\mathbf{z}^q$ —characterized by scores exceeding 90% of the samples — we observe that $s_{T<1} = 1$ and $s_{T>1} = 1$.

A.2 Proof of Proposition A.6

We start by stating and proving Lemmas A.7 and A.8, which serve as auxiliary to Proposition A.6.

Lemma A.7. *Let $\boldsymbol{\pi}$ be a descendingly sorted softmax vector and $\boldsymbol{\pi}_T$ the same vector after temperature scaling . Define the difference vector $\mathbf{d} := \boldsymbol{\pi} - \boldsymbol{\pi}_T$. Then, there exists an index such that the vector $\mathbf{d}$ is partitioned into two segments, where all elements in one segment have the opposite sign to those in the other segment.*

Proof. First, let us formulate this proposition:
Let $\mathbf{z} \in \mathbb{R}^C$ such that $z_1 \geq z_2 \geq \cdots \geq z_C$. Consider the following function difference:

$$d(\mathbf{z}; T, i) = \frac{\exp(z_i)}{\sum_{j=1}^{C} \exp(z_j)} - \frac{\exp(z_i/T)}{\sum_{j=1}^{C} \exp(z_j/T)} = \pi_i - \pi_{T,i}$$

The following holds:

$$\begin{cases} \text{If} \quad 0 < T < 1 \quad \text{and} \quad \exists i \in [C] \quad \text{s.t.} \quad d(\mathbf{z}; T, i) > 0: \quad \forall k > i \quad d(\mathbf{z}; T, k) > 0 \\ \text{If} \quad T > 1 \quad \text{and} \quad \exists i \in [C] \quad \text{s.t.} \quad d(\mathbf{z}; T, i) < 0: \quad \forall k > i \quad d(\mathbf{z}; T, k) < 0 \end{cases}$$

Denote $A := \frac{1}{\sum_{j=1}^{C} \exp(z_j)}$ and $B := \frac{1}{\sum_{j=1}^{C} \exp(z_j/T)}$. Notice that $\mathbf{z}$ and T are constants and only i is changing in the theorem condition. Let us rewrite $d(\mathbf{z}; T, i)$:

$$d(\mathbf{z}; T, i) = d(z_i) = A \exp(z_i) - B \exp(z_i/T)$$

Notice that $d(z_i)$ is a discrete function because $z_i \in \mathbf{z}$. To understand when is it possible that $d(z_i) = 0$ we convert the function to continuous, i.e., z_i can be any value. The continuous function (that gets single variable instead of vector) is as follows:

$$d(x) = A \exp(x) - B \exp(x/T)$$

There is a *single* solution of the equation $d(x) = 0$ which is $x = \frac{T}{T-1} \ln(B/A) := x^*$. We will now divide the rest of the proof into two temperature branches:

- **T > 1 branch:** Assume $x_1 < x^*, d(x_1) < 0$ then, $\forall x < x_1$ we have $d(x) < 0$.
  In our discrete case, we know that $d(z_1) > 0$ (substitute $L = 1$ in Theorem A.1), and that $d(z_i) < 0$ (therefore $z_i < z^*$ in our analogy to the continuous case), consequently $\forall z_k < z_i,\ d(z_k) < 0$. Overall, because $k > i$, $z_k < z_i$ and we get that $d(z; T, k) < 0$.
- **0 < T < 1 branch:** Assume $x_2 > x^*, d(x_2) > 0$ then, $\forall x > x_2$ we have $d(x) > 0$.
  In our discrete case, we know that $d(z_1) < 0$ (substitute $L = 1$ in Theorem A.1), and that $d(z_i) > 0$ (therefore $z_i < z^*$ in our analogy to the continuous case), consequently $\forall z_k < z_i,\ d(z_k) > 0$. Overall, because $k > i$, $z_k < z_i$ and we get that $d(z; T, k) > 0$.

□

Lemma A.8. *Let $\mathbf{z} \in \mathbb{R}^C$ such that $z_1 \geq z_2 \geq \cdots \geq z_C$. Consider the following functions:*

$$d(\mathbf{z}; T, i) = \frac{\exp(z_i)}{\sum_{j=1}^{C} \exp(z_j)} - \frac{\exp(z_i/T)}{\sum_{j=1}^{C} \exp(z_j/T)}$$

$$g(\mathbf{z}; T, M) = \frac{\sum_{i=1}^{M} \exp(z_i)}{\sum_{j=1}^{C} \exp(z_j)} - \frac{\sum_{i=1}^{M} \exp(z_i/T)}{\sum_{j=1}^{C} \exp(z_j/T)} = \sum_{i=1}^{M} d(\mathbf{z}; T, i)$$

Then, if we denote by $s_{T>1} = \max\{i \in [C] : d(\mathbf{z}; T, j) > 0\}$ the last index where $d(\mathbf{z}, T, \cdot)$ is positive and similarly by $s_{T<1} = \max\{i \in [C] : d(\mathbf{z}; T, j) < 0\}$ the last index where $d(\mathbf{z}, T, \cdot)$ is negative, the following holds:

$$\begin{cases} \textit{If} \quad 0 < T < 1: \quad \forall M, L^q \in [C] \quad |g(\mathbf{z}; T, M) - g(z; T, L^q)| < \left| \sum_{i=1}^{s_{T<1}} d(z^q; T, i) \right| \\ \textit{If} \quad T > 1: \quad \forall M, L^q \in [C] \quad |g(\mathbf{z}; T, M) - g(\mathbf{z}; T, L^q)| < \left| \sum_{i=1}^{s_{T>1}} d(z^q; T, i) \right| \end{cases}$$

Proof. Let us begin by rewriting $|g(\mathbf{z}; T, M) - g(\mathbf{z}; T, L^q)|$, assume $M > L^q$ without loss of generality:

$$\begin{aligned} |g(\mathbf{z}; T, M) - g(\mathbf{z}; T, L^q)| &= \left| \frac{\sum_{i=1}^{M} \exp(z_i)}{\sum_{j=1}^{C} \exp(z_j)} - \frac{\sum_{i=1}^{M} \exp(z_i/T)}{\sum_{j=1}^{C} \exp(z_j/T)} - \left(\frac{\sum_{i=1}^{L^q} \exp(z_i)}{\sum_{j=1}^{C} \exp(z_j)} - \frac{\sum_{i=1}^{L^q} \exp(z_i/T)}{\sum_{j=1}^{C} \exp(z_j/T)} \right) \right| \\ &= \left| \sum_{i=1}^{M} d(\mathbf{z}; T, i) - \sum_{i=1}^{L^q} d(\mathbf{z}; T, i) \right| = \left| \sum_{i=L^q+1}^{M} d(\mathbf{z}; T, i) \right| \end{aligned}$$

Henceforth we denote $s := s_{T>1}$ or $s := s_{T<1}$ depending on the temperature. By Lemma A.7, $\forall i < s$ we have $d(\mathbf{z}; T, i) > 0$ and $\forall i > s$ we have $d(\mathbf{z}; T, i) < 0$, therefore we can divide the analysis of $\left| \sum_{i=L^q+1}^{M} d(\mathbf{z}; T, i) \right|$ into 3 cases:

- $L^q + 1 \geq s$ - in this case, we sum only on differences with the same sign, and we can create an upper bound for this case by summing all the differences with the same sign:

$$\left| \sum_{i=L^q+1}^{M} d(\mathbf{z}; T, i) \right| \leq \left| \sum_{i=s+1}^{C} d(\mathbf{z}; T, i) \right|$$

- $M \leq s$ - in this case like previous case, we sum only on differences with the same sign, and we can create an upper bound for this case by summing all the differences with the same sign, note that in any case the starting index of the summation is 2 or higher ($L^q + 1 \geq 2$), therefore we can exclude the first difference:

$$\left| \sum_{i=L^q+1}^{M} d(\mathbf{z}; T, i) \right| \leq \left| \sum_{i=2}^{s} d(\mathbf{z}; T, i) \right|$$

- $L^q + 1 < s$ and $M > s$ - in this case, we sum both on positive and negative differences, and we can create an upper bound for this case by taking the maximum between previous cases bounds:

$$\left| \sum_{i=L^q+1}^{M} d(\mathbf{z}; T, i) \right| \leq \max \left\{ \left| \sum_{i=s+1}^{C} d(\mathbf{z}; T, i) \right|, \left| \sum_{i=2}^{s} d(\mathbf{z}; T, i) \right| \right\}$$

Overall , we can write the upper bound of $\left| \sum_{i=L^q+1}^{M} d(\mathbf{z}; T, i) \right|$ as in case 3:

$$\left| \sum_{i=L^q+1}^{M} d(\mathbf{z}; T, i) \right| \leq \max \left\{ \left| \sum_{i=s+1}^{C} d(\mathbf{z}; T, i) \right|, \left| \sum_{i=2}^{s} d(\mathbf{z}; T, i) \right| \right\}$$

Note that the summation of all differences is zero, I.e. $\sum_{i=1}^{C} d(\mathbf{z}; T, i) = 0$, therefore,

$\sum_{i=1}^{s} d(\mathbf{z}; T, i) = -\sum_{i=s+1}^{C} d(\mathbf{z}; T, i)$ and $\left| \sum_{i=1}^{s} d(\mathbf{z}; T, i) \right| = \left| \sum_{i=s+1}^{C} d(\mathbf{z}; T, i) \right|$. because both summations contain differences with the same sign, subtracting elements from them decrease them, therefore,

$$\left| \sum_{i=2}^{s} d(\mathbf{z}; T, i) \right| < \left| \sum_{i=s+1}^{C} d(\mathbf{z}; T, i) \right|$$

$$\Downarrow$$

$$\max \left\{ \left| \sum_{i=s+1}^{C} d(\mathbf{z}; T, i) \right|, \left| \sum_{i=2}^{s} d(\mathbf{z}; T, i) \right| \right\} = \left| \sum_{i=s+1}^{C} d(\mathbf{z}; T, i) \right| = \left| \sum_{i=1}^{s} d(\mathbf{z}; T, i) \right|$$

And overall we get:

$$\forall M, L^q \in [C] \quad |d(\mathbf{z}; T, M) - g(\mathbf{z}; T, L^q)| < \left| \sum_{i=1}^{s} d(\mathbf{z}; T, i) \right|$$

□

We now turn to proving Proposition A.6.

Proof. **T > 1 branch:**
Substituting $s = 1$ in Lemma A.8 we get:

$$\forall M, L^q \in [C] \quad |g(\mathbf{z}; T, M) - g(\mathbf{z}; T, L^q)| < \left| \sum_{i=1}^{s=1} d(\mathbf{z}; T, i) \right| = |d(\mathbf{z}; T, 1)| = d(\mathbf{z}; T, 1)$$

We can remove the absolute value because $d(\mathbf{z};T,1) > 0$ for $T > 1$.
We continue by bounding $d(\mathbf{z};T,1)$:

$$\begin{aligned} d(\mathbf{z};T,1) &= \frac{\exp(z_1)}{\sum_{j=1}^{C}\exp(z_j)} - \frac{\exp(z_1/T)}{\sum_{j=1}^{C}\exp(z_j/T)} < 1 - \frac{\exp(z_1/T)}{\sum_{j=1}^{C}\exp(z_j/T)} \\ &= 1 - \frac{\exp(z_1/T)}{\exp(z_1/T)\left[\sum_{j=2}^{C}\exp(-(z_1-z_j)/T)+1\right]} = 1 - \frac{1}{\sum_{j=2}^{C}\exp(-(z_1-z_j)/T)+1} \\ &\leq 1 - \frac{1}{(C-1)\exp(-\Delta z/T)+1} = \frac{(C-1)\exp(-\Delta z/T)}{(C-1)\exp(-\Delta)/T)+1} \end{aligned}$$

Overall, we get:

$$\forall M, L^q \in [C] \quad |g(\mathbf{z};T,M) - g(\mathbf{z};T,L^q)| < \frac{(C-1)\exp\left(-\Delta z/T\right)}{(C-1)\exp\left(-\Delta z/T\right)+1}$$

0 < T < 1 branch:
Substituting $s = 1$ in Lemma A.8 we get:

$$\forall M, L^q \in [C] \quad |g(\mathbf{z};T,M) - g(\mathbf{z};T,L^q)| < \left|\sum_{i=1}^{s=1} d(\mathbf{z};T,M)\right| = |d(\mathbf{z};T,1)| = -d(\mathbf{z};T,1)$$

We can remove the absolute value and add minus sign because $d(z;T,1) < 0$ for $T > 1$.
We continue by bounding $-d(\mathbf{z};T,1)$:

$$\begin{aligned} |d(\mathbf{z};T,1)| = -d(\mathbf{z};T,1) &= \frac{\exp(z_1/T)}{\sum_{j=1}^{C}\exp(z_j/T)} - \frac{\exp(z_1)}{\sum_{j=1}^{C}\exp(z_j)} < 1 - \frac{\exp(z_1)}{\sum_{j=1}^{C}\exp(z_j)} \\ &= 1 - \frac{\exp(z_1)}{\exp(z_1)\left[\sum_{j=2}^{C}\exp(-(z_1-z_j))+1\right]} = 1 - \frac{1}{\sum_{j=2}^{C}\exp(-(z_1-z_j))+1} \\ &\leq 1 - \frac{1}{(C-1)\exp(-\Delta z)+1} = \frac{(C-1)\exp(-\Delta z)}{(C-1)\exp(-\Delta z))+1} \end{aligned}$$

Overall, we get:

$$\forall M, L^q \in [C] \quad |g(\mathbf{z};T,M) - g(\mathbf{z};T,L^q)| < \frac{(C-1)\exp\left(-\Delta z\right)}{(C-1)\exp\left(-\Delta z\right)+1}$$

□

B Additional Experimental Details and Results

B.1 Training details

For ImageNet models, we utilized pretrained models from the `TORCHVISION.MODELS` sub-package. For full training details, please refer to the following link:

`https://github.com/pytorch/vision/tree/8317295c1d272e0ba7b2ce31e3fd2c048235fc73/references/classification`

For CIFAR-100 and CIFAR-10 models, we use: Batch size: 128; Epochs: 300; Cross-Entropy loss; Optimizer: SGD; Learning rate: 0.1; Momentum: 0.9; Weight decay: 0.0005.

B.2 Experiments compute resources

We conducted our experiments using an NVIDIA GeForce GTX 1080 Ti. Given the trained models, each experiment runtime is within a range of minutes.

B.3 Temperature scaling calibration

As mentioned in Section 2.1, two popular calibration objectives are the Negative Log-Likelihood (NLL) (Hastie et al., 2005) and the Expected Calibration Error (ECE) (Naeini et al., 2015).

NLL, given by $\mathcal{L} = -\sum_{i=1}^{n} \ln(\tilde{\pi}_{y_i}(\mathbf{x}_i))$, measures the cross-entropy between the true conditional distribution of data (one-hot vector associated with y_i) and $\tilde{\boldsymbol{\pi}}(\mathbf{x}_i)$.

ECE aims to approximate $\mathbb{E}\left[\left|\mathbb{P}\left(\hat{y}(X) = Y | \tilde{\pi}_{\hat{y}(X)}(X) = p\right) - p\right|\right]$. Specifically, the confidence range $[0, 1]$ is divided into L equally sized bins $\{B_l\}$. Each sample $(\mathbf{x}_i, y_i)$ is assigned to a bin B_l according to $\tilde{\pi}_{y_i}(\mathbf{x}_i)$. The objective is given by $\text{ECE} = \sum_{l=1}^{L} \frac{|B_l|}{n} \left|\text{acc}(B_l) - \text{conf}(B_l)\right|$, where $\text{acc}(B_l) = \frac{1}{|B_l|} \sum_{i \in B_l} \mathbb{1}\{\hat{y}(\mathbf{x}_i) = y_i\}$ and $\text{conf}(B_l) = \frac{1}{|B_l|} \sum_{i \in B_l} \hat{\pi}_{y_i}(\mathbf{x}_i)$. Here, $\mathbb{1}(\cdot)$ denotes the indicator function.

B.3.1 ECE vs NLL minimization

Above, we defined the two common minimization objectives for the TS calibration procedure. Throughout the paper, we employed the ECE objective. Here, we justify this choice by demonstrating the proximity of the optimal calibration temperature T^* for both objectives.

Table 3: Optimal Temperature for NLL and ECE objectives

Dataset-Model	T^* - NLL loss	T^* - ECE loss
CIFAR-100, ResNet50	1.438	1.524
CIFAR-100, DenseNet121	1.380	1.469
ImageNet, ResNet152	1.207	1.227
ImageNet, DenseNet121	1.054	1.024
ImageNet, ViT-B/16	1.18	1.21
CIFAR-10, ResNet50	1.683	1.761
CIFAR-10, ResNet34	1.715	1.802

Using both objectives, we obtain similar optimal calibration temperatures T^*, resulting in minor changes to the values in Tables 1 and 2, presented in Section 3.2. Furthermore, in Section 3.3, we examine the effect of TS over a range of temperatures, which naturally includes both optimal temperatures.

B.4 METRICS DEFINITIONS

In section 3.1, we use metrics to represent average prediction set size, marginal coverage and conditional coverage. Here, we present the formulas for these metrics. Note that similar metrics have been used in (Ding et al., 2023; Angelopoulos et al., 2021).

We report metrics over the validation set which we denote by $\{(X_i^{(val)}, Y_i^{(val)})\}_{i=1}^{N^{(val)}}$, comprising of the samples that were not included in the calibration set or CP set. The metrics are as follows.

- *Average set size* (AvgSize) – The mean prediction set size of the CP algorithm:

$$\text{AvgSize} = \frac{1}{N^{(val)}} \sum_{i=1}^{N^{(val)}} |C(X_i^{(val)})|. \tag{15}$$

- *Marginal coverage gap* (MarCovGAP) – The deviation of the marginal coverage from the desired $1-\alpha$:

$$\text{MarCovGap} = \left| \frac{1}{N^{(val)}} \sum_{i=1}^{N^{(val)}} \mathbb{1}\{Y_i^{(val)} \in C(X_i^{(val)})\} - (1-\alpha) \right|. \tag{16}$$

- *Top-5% class-coverage gap* (TopCovGap) – The deviation from the desired $1-\alpha$ coverage, averaged over the 5% of classes with the highest deviation:

$$\text{TopCovGap} = \text{Top5}_{y\in[C]} \left| \frac{1}{|I_y|} \sum_{i\in I_y} \mathbb{1}\left\{Y_i^{(val)} \in C\left(X_i^{(val)}\right)\right\} - (1-\alpha) \right|, \tag{17}$$

  where Top5 is an operator that returns the mean of the 5% highest elements in the set and $I_y = \{i \in [N^{(val)}] : Y_i^{(val)} = y\}$ is the indices of validation examples with label y. We use top-5% classes deviation due to the high variance in the maximal class deviation. For example, in CIFAR-100, the average is computed over the 5 classes with the highest deviation from $1-\alpha$ coverage. Thus, TopCovGap is a class-conditional coverage metric.

B.4.1 RELIABILITY DIAGRAMS

Below, we present reliability diagrams for dataset-model pairs examined in our study. We divided the confidence range into 10 bins and displayed the accuracy for each bin as a histogram. The red bars represent the calibration error for each bin.

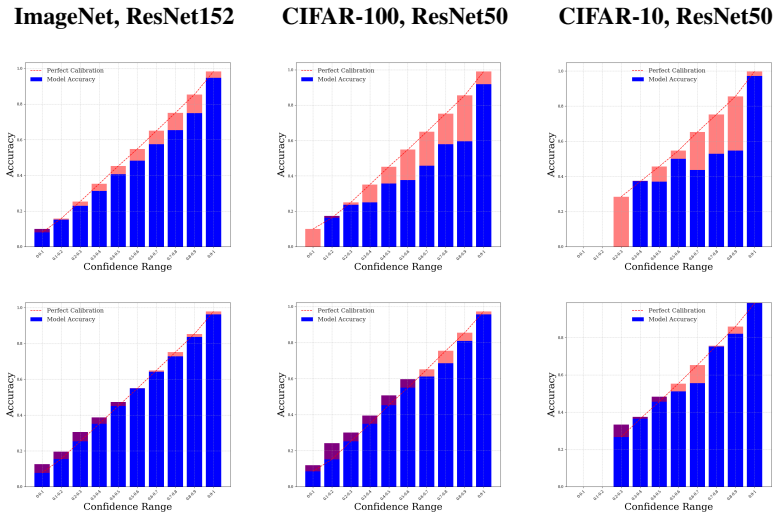

Figure 7: Reliability diagrams before (top) and after (bottom) TS calibration with ECE objective.

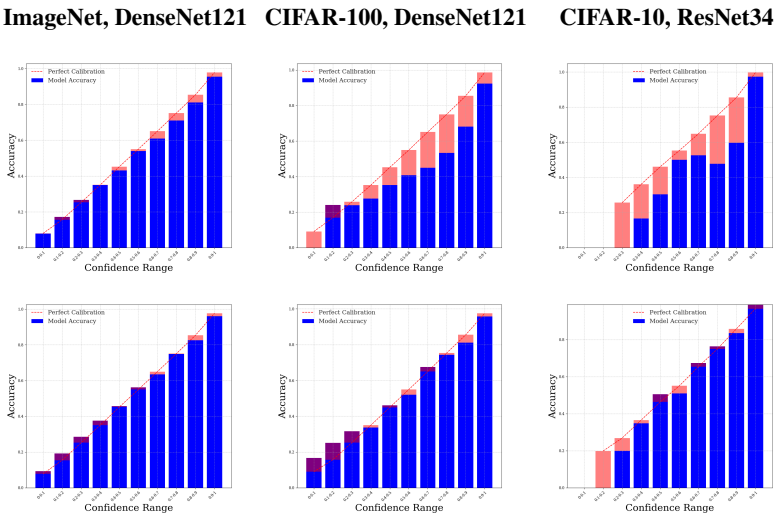

Figure 8: Reliability diagrams before (top) and after (bottom) TS calibration with ECE objective.

B.5 THE EFFECT OF TS CALIBRATION ON CP METHODS

As an extension of Section 3.2, we provide additional experiments where we examine the effect of TS calibration on CP methods with different settings of hyper-parameters (α and CP set size). The tables below present prediction set sizes and coverage metrics before and after TS calibration for different CP set sizes and an additional CP coverage probability value.

Table 4: **Prediction Set Size.** AvgSize metric along with T^* and accuracy for dataset-model pairs using LAC, APS, and RAPS algorithms with $\alpha = 0.1$, CP set size 5%, pre- and post-TS calibration.

		Accuracy(%)		**AvgSize**			**AvgSize after TS**		
Dataset-Model	T^*	Top-1	Top-5	LAC	APS	RAPS	LAC	APS	RAPS
ImageNet, ResNet152	1.227	78.3	94.0	1.94	7.24	3.20	1.95	10.3	4.35
ImageNet, DenseNet121	1.024	74.4	91.9	2.70	10.1	4.71	2.77	11.2	4.91
ImageNet, ViT-B/16	1.180	83.9	97.0	2.75	10.18	2.01	2.33	19.19	2.41
CIFAR-100, ResNet50	1.524	80.9	95.4	1.62	5.75	2.78	1.57	9.76	4.93
CIFAR-100, DenseNet121	1.469	76.1	93.5	2.10	4.30	2.99	2.08	6.61	4.38
CIFAR-10, ResNet50	1.761	94.6	99.7	0.92	1.05	0.95	0.91	1.13	1.01
CIFAR-10, ResNet34	1.802	95.3	99.8	0.91	1.03	0.94	0.93	1.11	1.05

Table 5: **Prediction Set Size.** AvgSize metric along with T^* and accuracy for dataset-model pairs using LAC, APS, and RAPS algorithms with $\alpha = 0.1$, CP set size 20%, pre- and post-TS calibration.

		Accuracy(%)		**AvgSize**			**AvgSize after TS**		
Dataset-Model	T^*	Top-1	Top-5	LAC	APS	RAPS	LAC	APS	RAPS
ImageNet, ResNet152	1.227	78.3	94.0	1.95	7.34	3.30	1.92	12.5	4.40
ImageNet, DenseNet121	1.024	74.4	91.9	2.73	13.1	4.70	2.76	13.3	4.88
ImageNet, ViT-B/16	1.180	83.9	97.0	2.69	10.03	1.89	2.24	19.05	2.48
CIFAR-100, ResNet50	1.524	80.9	95.4	1.62	5.35	2.68	1.57	9.34	4.96
CIFAR-100, DenseNet121	1.469	76.1	93.5	2.13	4.36	2.95	2.06	6.81	4.37
CIFAR-10, ResNet50	1.761	94.6	99.7	0.91	1.04	0.98	0.91	1.13	1.05
CIFAR-10, ResNet34	1.802	95.3	99.8	0.91	1.03	0.94	0.93	1.11	1.05

Table 6: **Coverage Metrics.** MarCovGap and TopCovGap metrics for dataset-model pairs using LAC, APS, and RAPS algorithms with $\alpha = 0.1$, CP set size 5%, pre- and post-TS calibration.

	MarCovGap(%)			**MarCovGap TS(%)**			**TopCovGap(%)**			**TopCovGap TS(%)**		
Dataset-Model	LAC	APS	RAPS	LAC	APS	RAPS	LAC	APS	RAPS	LAC	APS	RAPS
ImageNet, ResNet152	0	0	0	0	0.1	0	23.5	15.7	16.9	24.1	13.6	15.0
ImageNet, DenseNet121	0	0.1	0	0	0	0.1	24.9	15.7	18	25.2	14.9	17.6
ImageNet, ViT-B/16	0	0	0.1	0.1	0	0	24.1	14.9	14.5	24.8	12.4	12.6
CIFAR-100, ResNet50	0.1	0	0.1	0	0.1	0	13.9	11.9	10.7	12.5	8.2	7.5
CIFAR-100, DenseNet121	0	0	0.1	0	0	0.1	11.6	9.5	9.0	11.7	7.8	7.7
CIFAR-10, ResNet50	0	0	0	0	0.1	0	11.1	5.0	4.8	11.2	2.4	2.6
CIFAR-10, ResNet34	0	0.1	0.1	0	0	0	9.5	3.0	2.8	9.1	2.2	2.2

Table 7: **Coverage Metrics.** MarCovGap and TopCovGap metrics for dataset-model pairs using LAC, APS, and RAPS algorithms with $\alpha = 0.1$, CP set size 20%, pre- and post-TS calibration.

	MarCovGap(%)			**MarCovGap TS(%)**			**TopCovGap(%)**			**TopCovGap TS(%)**		
Dataset-Model	LAC	APS	RAPS	LAC	APS	RAPS	LAC	APS	RAPS	LAC	APS	RAPS
ImageNet, ResNet152	0.1	0.1	0	0.1	0	0	23.6	16.3	17.5	23.6	13.9	15.6
ImageNet, DenseNet121	0	0.1	0	0	0	0	24.9	15.7	18	25.2	14.9	17.6
ImageNet, ViT-B/16	0	0	0.1	0.1	0	0	23.9	15.2	14.1	24.3	12.7	12.6
CIFAR-100, ResNet50	0.1	0.1	0	0	0.1	0	11.4	9.9	10.0	13.0	7.7	8.2
CIFAR-100, DenseNet121	0	0	0	0	0	0.1	11.5	9.5	9.7	12.2	7.8	8.0
CIFAR-10, ResNet50	0	0	0	0	0.1	0	10.8	5.1	4.6	11.0	2.1	2.6
CIFAR-10, ResNet34	0	0	0.1	0	0	0	9.1	3.1	2.6	9.3	2.1	2.3

We can see from the above tables that the results for different CP sizes are very similar. The goal of the CP set is to be large enough to represent the rest of the data from the same distribution. In our experiments, we see that even 5% of the validation set is sufficient for this purpose.

The increased coverage probability is reflected in both prediction set sizes and the conditional coverage metric. We observe an increase in prediction set sizes compared to Table 1, which is expected due to the stricter coverage probability requirement. Note that the tendency for prediction set sizes to

Table 8: **Prediction Set Size.** AvgSize metric along with T^* and accuracy for dataset-model pairs using LAC, APS, and RAPS algorithms with $\alpha = 0.05$, CP set size 10%, pre- and post-TS calibration.

		Accuracy(%)		**AvgSize**			**AvgSize after TS**		
Dataset-Model	T^*	Top-1	Top-5	LAC	APS	RAPS	LAC	APS	RAPS
ImageNet, ResNet152	1.227	78.3	94.0	3.28	14.9	4.10	3.22	24.1	5.1
ImageNet, DenseNet121	1.024	74.4	91.9	3.33	20.1	5.02	3.61	22.8	5.88
ImageNet, ViT-B/16	1.180	83.9	97.0	2.91	22.80	4.51	3.02	39.8	5.55
CIFAR-100, ResNet50	1.524	80.9	95.4	3.97	11.10	3.98	2.21	16.2	6.80
CIFAR-100, DenseNet121	1.469	76.1	93.5	4.89	8.81	5.01	4.23	12.16	6.11
CIFAR-10, ResNet50	1.761	94.6	99.7	1.02	1.08	1.08	1.02	1.21	1.21
CIFAR-10, ResNet34	1.802	95.3	99.8	1.01	1.06	1.19	1.01	1.06	1.19

Table 9: **Coverage Metrics.** MarCovGap and TopCovGap metrics for dataset-model pairs using LAC, APS, and RAPS algorithms with $\alpha = 0.05$, CP set size 10%, pre- and post-TS calibration.

	MarCovGap(%)			**MarCovGap TS(%)**			**TopCovGap(%)**			**TopCovGap TS(%)**		
Dataset-Model	LAC	APS	RAPS	LAC	APS	RAPS	LAC	APS	RAPS	LAC	APS	RAPS
ImageNet, ResNet152	0.1	0	0	0	0	0	16.1	11.5	14.3	16.5	10.1	12.4
ImageNet, DenseNet121	0	0.1	0	0.1	0	0	15.5	12.0	15.0	16.0	11.7	14.3
ImageNet, ViT-B/16	0.1	0	0	0	0.1	0.1	14.6	11.6	11.5	15.0	9.27	9.78
CIFAR-100, ResNet50	0.1	0	0	0	0.1	0	7.51	8.81	6.82	7.28	4.9	4.48
CIFAR-100, DenseNet121	0	0	0	0	0	0.1	6.72	5.91	6.50	6.50	5.41	5.41
CIFAR-10, ResNet50	0	0	0	0	0.1	0	6.50	4.22	4.22	7.03	2.13	1.98
CIFAR-10, ResNet34	0	0	0.1	0	0	0	4.12	2.71	2.73	4.17	1.27	1.29

increase with T remains. Regarding the coverage metric TopCovGap, we see an improvement (lower values), which can be explained by the increase in prediction set sizes. Here, the tendency for the metrics to improve as T increases also remains.

In addition to the tables, in Section 3.2, we microscopically investigated the effect of TS calibration on PS sizes. Figure 1 represents the sorted differences in prediction set sizes for each sample in the validation set for CIFAR100-ResNet50. Here, in Figure 9, we provide similar figures for additional dataset-model pairs.

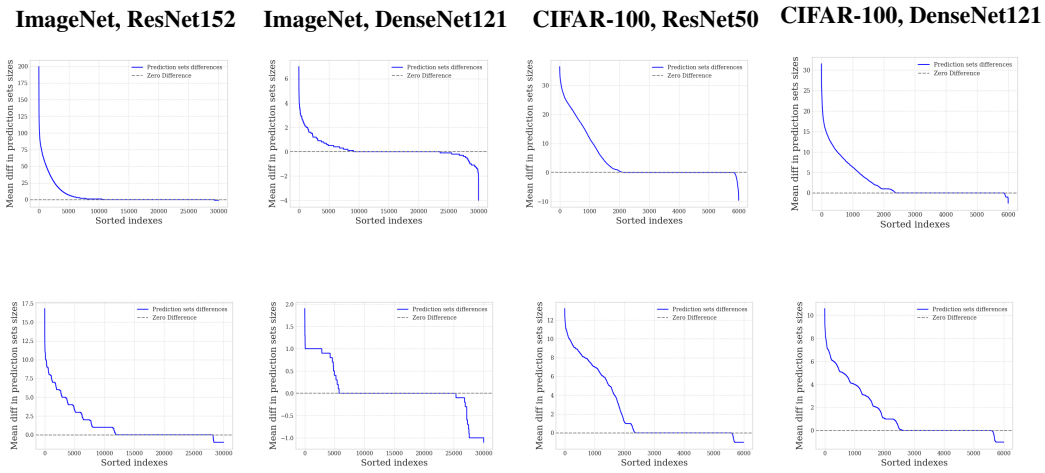

Figure 9: Mean sorted differences in prediction set sizes before and after TS calibration for APS (top) and RAPS (bottom) CP algorithms with $\alpha = 0.1$ and CP set size 10%.

B.6 TS BEYOND CALIBRATION

As an extension of Section 3.3, we provide additional experiments with different settings to examine the effect of TS beyond calibration on CP methods. The figures below present prediction set sizes and conditional coverage metrics for a range of temperatures for additional dataset-model pairs, different CP set sizes and an additional CP coverage probability value. Overall, the temperature T allows to trade off between AvgSize and TopCovGap, as discussed in the paper.

B.6.1 PREDICTION SET SIZE

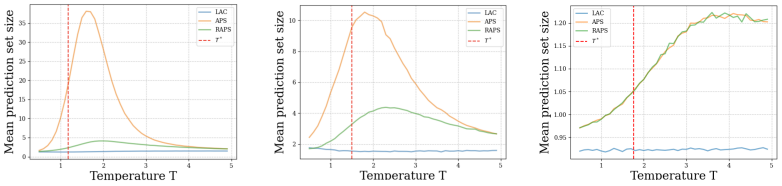

ImageNet, ViT-B/16 | CIFAR-100, ResNet50 | CIFAR-10, ResNet50

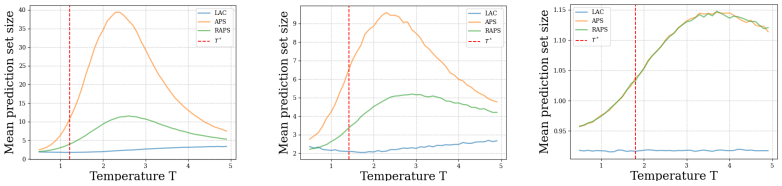

ImageNet, ResNet152 | CIFAR-100, DenseNet121 | CIFAR-10, ResNet34

Figure 10: **Prediction Set Size.** AvgSize using LAC, APS and RAPS with $\alpha = 0.1$ and CP set size 10% versus the temperature T for additional dataset-model pairs.

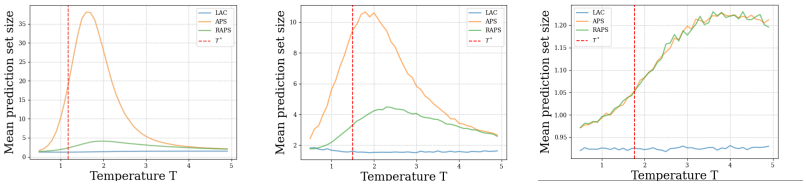

ImageNet, ViT-B/16 | CIFAR-100, ResNet50 | CIFAR-10, ResNet50

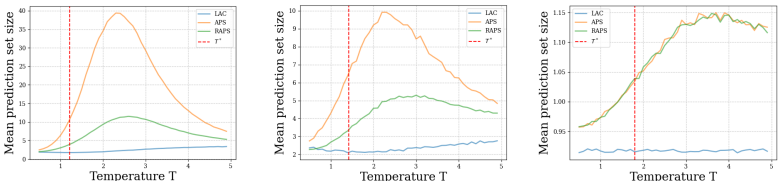

ImageNet, ResNet152 | CIFAR-100, DenseNet121 | CIFAR-10, ResNet34

Figure 11: **Prediction Set Size.** AvgSize using LAC, APS and RAPS with $\alpha = 0.1$ and CP set size 5%, versus the temperature T for additional dataset-model pairs.

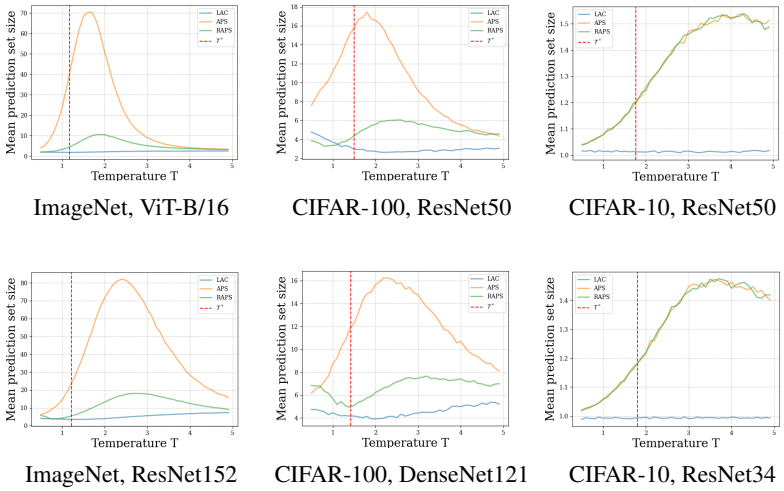

ImageNet, ViT-B/16 CIFAR-100, ResNet50 CIFAR-10, ResNet50

ImageNet, ResNet152 CIFAR-100, DenseNet121 CIFAR-10, ResNet34

Figure 12: **Prediction Set Size.** AvgSize using LAC, APS and RAPS with $\alpha = 0.05$ and CP set size 10% versus the temperature T for additional dataset-model pairs.

B.6.2 TopCovGap metric

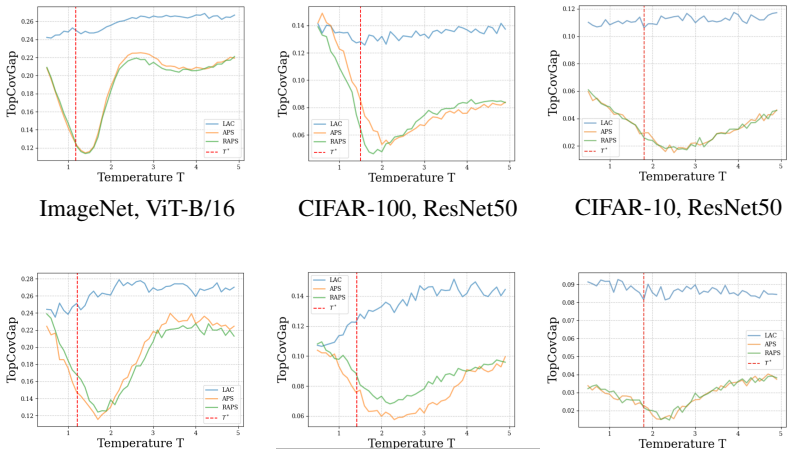

ImageNet, ViT-B/16 CIFAR-100, ResNet50 CIFAR-10, ResNet50

ImageNet, ResNet152 CIFAR-100, DenseNet121 CIFAR-10, ResNet34

Figure 13: **Conditional Coverage Metric.** TopCovGap using LAC, APS and RAPS with $\alpha = 0.1$ and CP set size 10% versus the temperature T for additional dataset-model pairs.

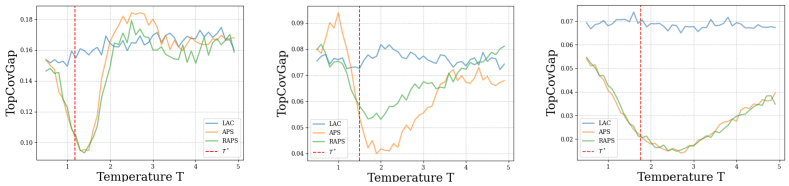

ImageNet, ViT-B/16 CIFAR-100, ResNet50 CIFAR-10, ResNet50

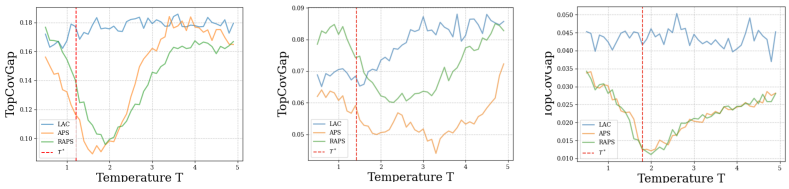

ImageNet, ResNet152 CIFAR-100, DenseNet121 CIFAR-10, ResNet34

Figure 14: **Conditional Coverage Metric.** TopCovGap using LAC, APS and RAPS with $\alpha = 0.05$ and CP set size 10% versus the temperature T for additional dataset-model pairs.

B.6.3 CP THRESHOLD VALUE $\hat{q}$

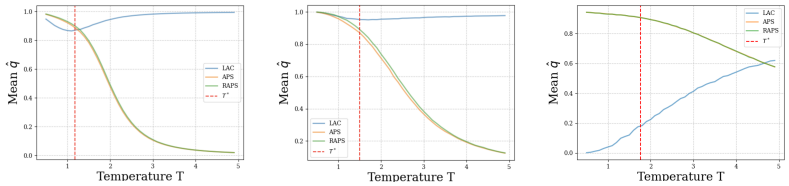

ImageNet, ViT-B/16 CIFAR-100, ResNet50 CIFAR-10, ResNet50

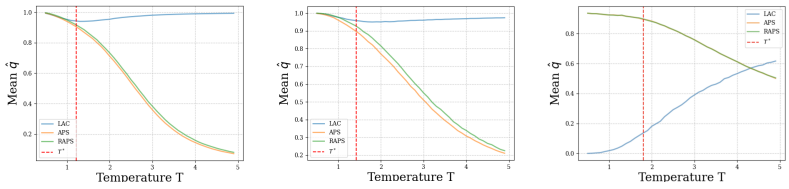

ImageNet, ResNet152 CIFAR-100, DenseNet121 CIFAR-10, ResNet34

Figure 15: **CP threshold value** $\hat{q}$ using LAC, APS and RAPS with $\alpha = 0.1$ and CP set size 10% versus the temperature T for additional dataset-model pairs.

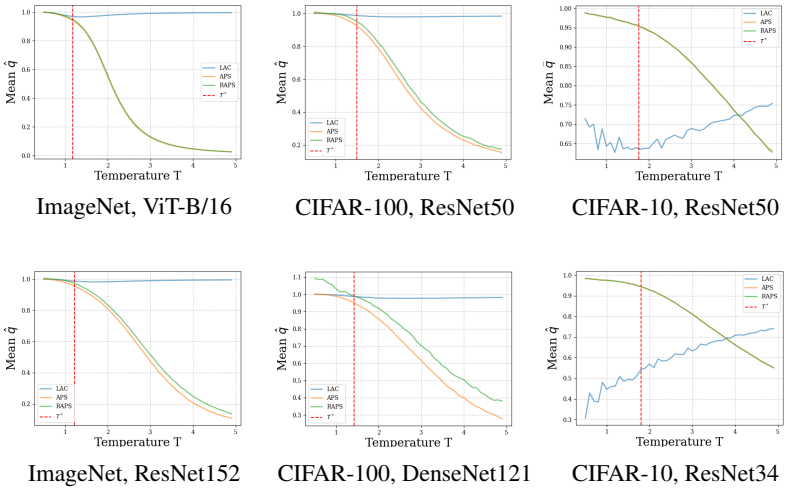

ImageNet, ViT-B/16 | CIFAR-100, ResNet50 | CIFAR-10, ResNet50

ImageNet, ResNet152 | CIFAR-100, DenseNet121 | CIFAR-10, ResNet34

Figure 16: **CP threshold value** $\hat{q}$ using LAC, APS and RAPS with $\alpha = 0.05$ and CP set size 10% versus the temperature T for additional dataset-model pairs.

B.6.4 The impact of TS at extremely low temperatures

In our experiments presented in Section 2, we lower bound the temperature range at $T = 0.3$. This choice was motivated by the deviation from the desired marginal coverage guarantee observed at extremely small temperatures. Specifically, we observe that for too small T the threshold value reaches maximal value, $\hat{q} \to 1$, and, presumably due to numerical errors, this leads to an impractical CP procedure, with significant over-coverage and excessively large prediction set sizes, as demonstrated in Figure 17 for CIFAR100-DenseNet121, $\alpha = 0.1$ and CP set size 10%.

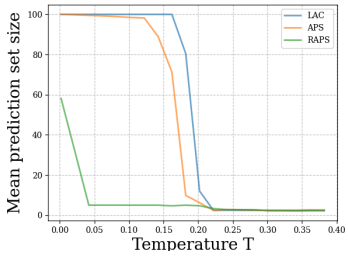

Figure 17: **Prediction Set Size.** Mean prediction set size for LAC, APS and RAPS versus low temperatures, for CIFAR100-DenseNet121.

C Approximating the Trade-off via the Calibration Set

As discussed in Section 5, exploring the trade-off between prediction set size and class-conditional coverage through the temperature parameter $\hat{T}$ is beneficial when using adaptive CP algorithms.

We propose using TS with two separate temperature parameters on distinct branches: T^*, optimized for TS calibration, and $\hat{T}$, which allows for trading prediction set sizes and conditional coverage properties of APS/RAPS to align better with task requirements. One limitation is that the metrics' values for different $\hat{T}$ are not known a priori. However, since we decouple calibration from the CP procedure, the calibration set can be used to evaluate CP algorithms without compromising exchangeability.

The curves in Figure 2 were generated by evaluating the CP methods on the entire validation set (excluding the calibration set and CP set) and averaging over 100 trials. Both are not feasible in practice, where the practitioner only has the calibration set and the CP set of a single trial. Here, we show that these curves can be approximated using only the calibration set for evaluation. In Figure 18, we plot the curves using calibration set + CP set, which together are 20% of the validation set (as in the main body of the paper). Specifically, 10% of the validation set is used for the CP operation (computing the threshold), and the remaining 10% (the original calibration set) serves as a "validation set" to evaluate the CP performance. Therefore, no additional samples are used compared to the common practice of performing calibration and CP calibration sequentially rather than in parallel.

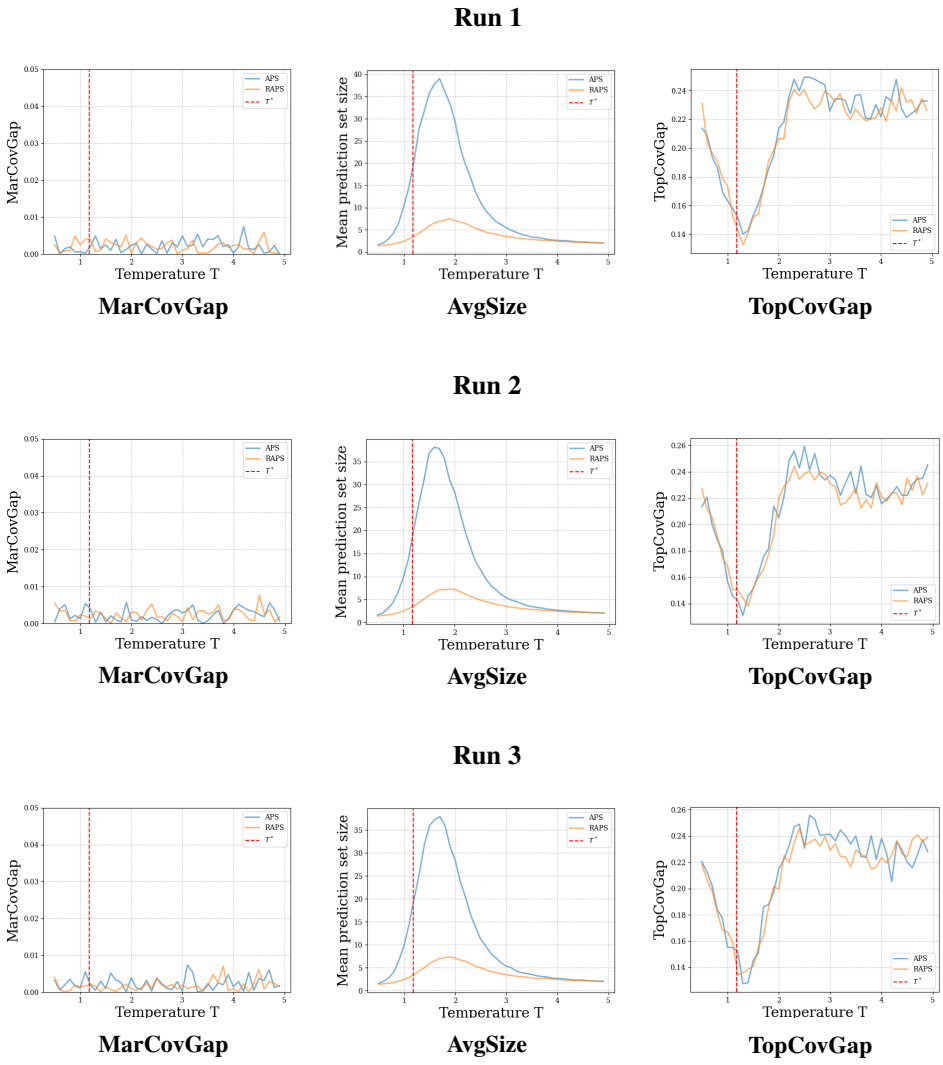

Figure 18: **Performance evaluation with small data.** Examining the performance of APS and RAPS with small evaluation data for ImageNet-ViT-B/16 with $\alpha = 0.1$ and CP set size 10%. Each row displays the marginal coverage, prediction size and conditional coverage metrics that are computed over 1 trial using 10% of the validation set.

Unlike the curves in Figure 2, the curves in Figure 18 are not averaged over 100 trials but are based on a single trial. Due to randomization, the curves will vary between runs, so to better reflect the practitioner's experience, we present results from 3 separate runs. In each of the runs in Figure 18 the marginal coverage is preserved and the curves of AvgSize and TopCovGap closely resemble the averaged ones shown in Figure 2, demonstrating the user's ability to select $\hat{T}$ based on these single-trial graphs generated using small amount of data. Additionally, note that the procedure required to produce these approximated curves is executed offline during calibration and has a negligible runtime compared to the offline training of DNNs.

D Advantages of the Proposed Guidelines over Mondrian Conformal Prediction

In this section, we consider the case of a user that prioritizes class-conditional coverage. In this case, our study recommends applying TS with $T_{critical}$ followed by an adaptive CP method like RAPS. Recall that using TS with $T_{critical}$ yields high AvgSize, but by the trade-off TopCovGap is low.

Table 10: Comparison between MCP vs TS with $T_{critical}$, both based on RAPS, for CIFAR100-ResNet50 and ImageNet-ViT.

	CIFAR100-ResNet50				**ImageNet-ViT**			
	MCP		**TS**		**MCP**		**TS**	
Metric \ CP set size (%)	10%	20%	10%	20%	10%	20%	10%	20%
AvgSize	5.5	4.2	4.2	4.1	NA	5.1	2.6	2.7
MarCovGap	0.04	0.02	0.00	0.00	NA	0.03	0.00	0.00
TopCovGap	0.28	0.20	0.08	0.08	NA	0.28	0.15	0.14

An existing alternative is to use the Mondrian Conformal Prediction (MCP) approach (Vovk, 2012). MCP aims to construct prediction sets with group-conditional coverage guarantees. Considering the groups to be the classes, the method is based on partitioning the data used for calibration (i.e., the CP set) by classes and obtaining a threshold per class. At deployment, the thresholds are used in a classwise manner. However, a major drawback of MCP is its limited applicability to classification tasks with many classes, since its performance degrades when the number of samples used for calibrating CP per class is small (Ding et al., 2023).

Note that in our experiments, we consider CIFAR-100 that has 100 classes and CP set (used to calibrate the CP) of size up to 2000 (20% of the validation set), and ImageNet that has 1000 classes and CP set of size up to 10000 (20% of the validation set). This means that, approximately, we have up to 20 samples per class to calibrate CP for CIFAR-100 and up to 10 samples per class to calibrate CP for ImageNet.

Table 10 presents the metrics AvgSize, MarCovGap and TopCovGap for our proposed approach and for MCP, when both utilize RAPS, for the dataset-model pairs CIFAR100-ResNet50 and ImageNet-ViT. "NA" indicates the inability to compute the metric, which occurs in this case due to the absence of samples for certain classes in the CP set (samples in the CP set are chosen randomly at each of the 100 trials), making it impossible to determine thresholds for those classes.

The results demonstrate the superiority of using TS with $T = T_{critical}$ (computed based on Theorem 4.4) over MCP across all metrics. Recall that we consider the case where class-conditional coverage is preferred, and indeed, TS with $T = T_{critical}$ constantly yields better TopCovGap than MCP. Yet, interestingly, it outperforms MCP also at AvgSize.

To conclude, the experiments presented in this section further shows the practical significance of our guidelines.